IN THE UNITED STATES PATENT AND TRADEMARK OFFICE

BEFORE THE PATENT TRIAL AND APPEAL BOARD

NOKIA OF AMERICA CORPORATION, ERICSSON INC., AT&T MOBILITY LLC, CELLCO PARTNERSHIP D/B/A/ VERIZON WIRELESS AND T-MOBILE USA, INC.,
Petitioners,

v.

SMART RF INC.,
Patent Owner.

U.S. Patent No. 9,641,204
Issue Date: May 2, 2017

DIGITAL MULTI-BAND PREDISTORTION LINEARIZER WITH NONLINEAR SUBSAMPLING ALGORITHM IN THE FEEDBACK LOOP

Inter Partes Review No.: IPR2025-00692

DECLARATION OF JUNE ANN MUNFORD

I. Introduction

I, June Ann Munford, do declare as follows:

1. I am over the age of 18, have personal knowledge of the facts set forth herein, and am competent to testify to the same.
2. I have been retained on behalf of the Petitioners to provide assistance in the above-identified matter in establishing the authenticity and public availability of the documents discussed in this declaration. I am being compensated for my services in this matter at the rate of $200.00 per hour plus reasonable expenses. My statements are objective, and my compensation does not depend on the outcome of this matter, the results of my study, or the substance of my opinions.

II. Qualifications and Professional Experience

3. I earned a Master of Library and Information Science (MLIS) from the University of Wisconsin-Milwaukee in 2009. I have over ten years of experience in the library/information science field. Beginning in 2004, I have served in various positions in the public library sector including Assistant Librarian, Youth Services Librarian and Library Director. I have attached my Curriculum Vitae as Appendix CV.
4. During my career in the library profession, I have been responsible for materials acquisition for multiple libraries. In that position, I have cataloged,

Exhibit 1007
Nokia of America Corporation, et al. v. Smart RF Inc.
000002

purchased, and processed incoming library works. That includes purchasing materials directly from vendors, recording publishing data from the material in question, creating detailed material records for library catalogs and physically preparing that material for circulation. In addition to my experience in acquisitions, I was also responsible for analyzing large collections of library materials, tailoring library records for optimal catalog search performance and creating lending agreements between libraries during my time as a Library Director.

5. I am fully familiar with the catalog record creation process in the library sector. In preparing a material for public availability, a library catalog record describing that material would be created. These records are typically written in Machine Readable Catalog (herein referred to as "MARC") code and contain information such as a physical description of the material, metadata from the material's publisher, and date of library acquisition. In particular, the 008 field of the MARC record is reserved for denoting the date of creation of the library record itself. As this typically occurs during the process of preparing materials for public access, it is my experience that an item's MARC record indicates the date of an item's public availability.
6. Typically, in creating a MARC record, a librarian would gather various bits of metadata such as book title, publisher and subject headings among others

and assign each value to a relevant numerical field. For example, a book's physical description is tracked in field 300 while title/attribution is tracked in field 245. The 008 field of the MARC record is reserved for denoting the creation of the library record itself, as I noted above. As this is the only date reflecting the inclusion of said materials within the library's collection, it is my experience that an item's 008 field accurately indicates the date of an item's public availability.

III. Authenticity and Public Availability (EX-1006)

A. Authentication

7. I have reviewed EX-1006, "A New Approach for Concurrent Dual-Band IF Digital PreDistortion: System Design and Analysis" by A. Cidronali, et al. as published in Proceedings of the 2008 International Workshop on Integrated Nonlinear Microwave and Millimeterwave Circuits (hereinafter, "Cidronali" or "EX-1006").

8. Attached hereto as Appendix CIDRONALI01 is a screen capture of a webpage entitled A New Approach for Concurrent Dual-Band IF Digital PreDistortion: System Design and Analysis as hosted on the IEEE Xplore website. I secured these screen captures myself from https://ieeexplore.ieee.org/document/4745733/metrics#metrics. Appendix CIDRONALI01 also contains a true and correct copy of Cidronali— "A

New Approach for Concurrent Dual-Band IF Digital PreDistortion: System Design and Analysis"—that I purchased from IEEE Xplore.

9. In comparing Appendix CIDRONALI01 to EX-1006, it is my determination that EX-1006 is a true and correct copy of "A New Approach for Concurrent Dual-Band IF Digital PreDistortion: System Design and Analysis" by A. Cidronali, et al. as published in Proceedings of the 2008 International Workshop on Integrated Nonlinear Microwave and Millimeterwave Circuits.

B. Public Availability

10. I am informed by counsel that a given reference is "published" upon a satisfactory showing that such a document has been disseminated or otherwise made publicly available to the extent that persons interested and ordinarily skilled in the subject matter or art could locate it exercising reasonable diligence and obtain the document. I have also been informed by counsel that materials available in a library constitute "printed publications" if they are catalogued and indexed according to general library practices and protocols that make the references available and accessible to members of the interested public.

1. <u>IEEE Xplore</u>

11. Appendix CIDRONALI01 as noted above is a screen capture of a webpage entitled "A New Approach for Concurrent Dual-Band IF Digital

PreDistortion: System Design and Analysis" as hosted on the IEEE Xplore website. The 'Date of Conference' field present in CIDRONALI01 indicates the conference associated with the Cidronali paper was held from November 24 – 25, 2008, and the 'Date Added to IEEE Xplore' field indicates the Cidronali paper was added to the IEEE Xplore online service as of January 9, 2009. Considering this information, it is my determination that Cidronali (EX-1006) was made available to the public via IEEE Xplore as of January 9, 2009.

2. Rochester Institute of Technology Library ("RIT")

12. Attached hereto as Appendix CIDRONALI02 is a true and correct copy of the MARC record for Proceedings of the 2008 International Workshop on Integrated Nonlinear Microwave and Millimeterwave Circuits as held by the Rochester Institute of Technology Library. I secured this record myself from the library's public catalog. The MARC record contained within Appendix CIDRONALI02 accurately describes the title, publisher and ISBN number of Proceedings of the 2008 International Workshop on Integrated Nonlinear Microwave and Millimeterwave Circuits.

13. The 008 field of the MARC record in Appendix CIDRONALI02 indicates the date of record creation. The 008 field of Appendix CIDRONALI02 indicates the Rochester Institute of Technology Library first acquired

Exhibit 1007
Nokia of America Corporation, et al. v. Smart RF Inc.
000006

Proceedings of the 2008 International Workshop on Integrated Nonlinear Microwave and Millimeterwave Circuits as of April 14, 2009. Considering this information, it is my determination that Proceedings of the 2008 International Workshop on Integrated Nonlinear Microwave and Millimeterwave Circuits, and therefore Cidronali (EX-1006), was made available to the public via the Rochester Institute of Technology Library shortly after April 14, 2009.

14. Additionally, subjects are represented in Field 050 by a Library of Congress Classification (LCC) number of "TK7871.58.P6" that represents general works on Amplifiers, specifically "Power." Subjects are also represented in Fields 650 by three Library of Congress subject headings: Power amplifiers, Microwave integrated circuits, and Millimeter wave devices. These subject representations support interested users to conduct subject searches to discover Cidronali (EX-1006).

3. MIT

15. Attached hereto as Appendix CIDRONALI03 is a true and correct copy of the MARC record for Proceedings of the 2008 International Workshop on Integrated Nonlinear Microwave and Millimeterwave Circuits as held by the Massachusetts Institute of Technology Library. I secured this record myself from the library's public catalog. The MARC record contained within

Exhibit 1007
Nokia of America Corporation, et al. v. Smart RF Inc.
000007

Appendix CIDRONALI03 accurately describes the title, publisher and ISBN number of Proceedings of the 2008 International Workshop on Integrated Nonlinear Microwave and Millimeterwave Circuits.

16. The 008 field of the MARC record in Appendix CIDRONALI03 indicates the date of record creation. The 008 field of Appendix CIDRONALI03 indicates the Massachusetts Institute of Technology Library first acquired Proceedings of the 2008 International Workshop on Integrated Nonlinear Microwave and Millimeterwave Circuits, as of April 14, 2009. Considering this information, it is my determination that Proceedings of the 2008 International Workshop on Integrated Nonlinear Microwave and Millimeterwave Circuits, and therefore Cidronali (EX-1006), was made available to the public via the Massachusetts Institute of Technology Library shortly after April 14, 2009.

17. Additionally, subjects are represented in Field 050 by a Library of Congress Classification (LCC) number of "TK7871.58" that represents general works on Amplifiers, specifically Power. Subjects are also represented in Fields 650 by three Library of Congress subject headings: Power amplifiers, Microwave integrated circuits and Millimeter wave devices. These subject representations support interested users to conduct subject searches to discover Cidronali (EX-1006).

4. Villanova

18. Attached hereto as Appendix CIDRONALI04 is a true and correct copy of the MARC record for Proceedings of the 2008 International Workshop on Integrated Nonlinear Microwave and Millimeterwave Circuits as held by the Villanova University Library. I secured this record myself from the library's public catalog. The MARC record contained within Appendix CIDRONALI04 accurately describes the title, publisher and ISBN number of Proceedings of the 2008 International Workshop on Integrated Nonlinear Microwave and Millimeterwave Circuits.

19. The 008 field of the MARC record in Appendix CIDRONALI04 indicates the date of record creation. The 008 field of Appendix CIDRONALI04 indicates the Villanova University Library first acquired Proceedings of the 2008 International Workshop on Integrated Nonlinear Microwave and Millimeterwave Circuits as of April 14, 2009. Considering this information, it is my determination that Proceedings of the 2008 International Workshop on Integrated Nonlinear Microwave and Millimeterwave Circuits, and therefore Cidronali (EX-1006), was made available to the public via Villanova University Library shortly after April 14, 2009.

20. Additionally, subjects are represented in Field 050 by a Library of Congress

Exhibit 1007
Nokia of America Corporation, et al. v. Smart RF Inc.
000009

Classification (LCC) number of "TK7871.58" that represents general works in Elctrical Engineering, Electronics and Nuclear Engineering, specifically on Power Amplifiers. Subjects are also represented in Fields 650 by three Library of Congress subject headings: Power amplifiers, Microwave integrated circuits and Millimeter wave devices Wireless communication systems. These subject representations support interested users to conduct subject searches to discover Cidronali (EX-1006).

5. Usage Record

21. Actual usage of a publication is reflected by other publications that make reference to it. I used Google Scholar to identify citations to Cidronali (EX-1006) and compiled a list of citations from 2009 through 2010. Appendix CIDRONALI05 presents 1 citation to this article. The earliest citation that I identified appeared in April 2010, further supporting my opinion that Cidronali (EX-1006) was made available to interested members of the public before April 2010 so that it could be cited in a paper published in April 2010.

22. Attached hereto as Appendix CIDRONALI06 is a chapter from a book entitled *Advanced Microwave Circuits and Systems*. I secured this chapter from the publisher's website at https://www.intechopen.com/chapters/9643. According to this page, *Advanced Microwave Circuits and Systems* was first published as of April 1, 2010. Page 36 of this chapter includes a citation to

Cidronali (EX-1006), indicating this reference was made available to interested members of the public before April 1, 2010 so that it could be cited in a textbook published on that date.

IV. Summary of My Opinion

23. My comparison of CIDRONALI01 to EX-1006 informs my opinion that EX-1006 is authentic. Based on the documents and records I have reviewed, it is my opinion that Cidronali (EX-1006)—*Proceedings of the 2008 International Workshop on Integrated Nonlinear Microwave and Millimeterwave Circuits*—was publicly accessible to interested members of the public via IEEE explore on the Internet by January 9, 2009. Further, the MARC records from the RIT, MIT, and Villanova Libraries show that the conference proceedings containing the Cidronali paper were catalogued and had a MARC record created on April 14, 2009. Based upon my experience and expertise, this confirms that Cidronali (EX-1006) would have been available to interested members of the public at each of these respective Libraries shortly after April 14, 2009, but not later than 2 – 12 weeks after the creation of the record. Further still, the citation history of Cidronali (EX-1006) confirms that by no later than April 1, 2010, interested members of the public had indeed accessed the Cidronali paper so that it could be cited in other publicly available works.

Exhibit 1007
Nokia of America Corporation, et al. v. Smart RF Inc.
000011

24. In sum, it is my opinion that persons interested and ordinarily skilled in the subject matter of the Cidronali paper would have been able to locate EX-1006 on the Internet by January 9, 2009, and certainly no later than April 1, 2010, based upon Cidronali's citation history.

25. I declare under penalty of perjury that the foregoing is true and correct. I hereby declare that all statements made herein of my own knowledge are true and that all statements made on information and belief are believed to be true; and further that these statements were made the knowledge that willful false statements and the like so made are punishable by fine or imprisonment, or both, under Section 1001 of Title 18 of the United States Code.

Dated: 3/7/2025

June Ann Munford

APPENDIX CV

June A. Munford
Curriculum Vitae

Education

University of Wisconsin-Milwaukee - MS, Library & Information Science, 2009
Milwaukee, WI

- Coursework included cataloging, metadata, data analysis, library systems, management strategies and collection development.
- Specialized in library advocacy, cataloging and public administration.

Grand Valley State University - BA, English Language & Literature, 2008
Allendale, MI

- Coursework included linguistics, documentation and literary analysis.
- Minor in political science with a focus in local-level economics and government.

Professional Experience

Researcher / Expert Witness, October 2017 – present
Freelance ● Pittsburgh, Pennsylvania & Grand Rapids, Michigan

- Material authentication and public accessibility determination. Declarations of authenticity and/or public accessibility provided upon research completion. Experienced with appeals and deposition process.

- Research provided on topics of public library operations, material publication history, digital database services and legacy web resources.

- Past clients include Alston & Bird, Arnold & Porter, Baker Botts, Fish & Richardson, Erise IP, Irell & Manella, O'Melveny & Myers, Perkins-Coie, Pillsbury Winthrop Shaw Pittman and Slayden Grubert Beard.

Library Director, February 2013 - March 2015
Dowagiac District Library ● Dowagiac, Michigan

- Executive administrator of the Dowagiac District Library. Located in

Southwest Michigan, this library has a service area of 13,000, an annual operating budget of over $400,000 and total assets of approximately $1,300,000.

● Developed careful budgeting guidelines to produce a 15% surplus during the 2013-2014 & 2014-2015 fiscal years while being audited.

● Using this budget surplus, oversaw significant library investments including the purchase of property for a future building site, demolition of existing buildings and building renovation projects on the current facility.

● Led the organization and digitization of the library's archival records.

● Served as the public representative for the library, developing business relationships with local school, museum and tribal government entities.

● Developed an objective-based analysis system for measuring library services - including a full collection analysis of the library's 50,000+ circulating items and their records.

November 2010 - January 2013
Librarian & Branch Manager, Anchorage Public Library ● Anchorage, Alaska

● Headed the 2013 Anchorage Reads community reading campaign including event planning, staging public performances and creating marketing materials for mass distribution.

● Co-led the social media department of the library's marketing team, drafting social media guidelines, creating original content and instituting long-term planning via content calendars.

● Developed business relationships with The Boys & Girls Club, Anchorage School District and the US Army to establish summer reading programs for children.

June 2004 - September 2005, September 2006 - October 2013
Library Assistant, Hart Area Public Library
Hart, MI

● Responsible for verifying imported MARC records and original MARC

cataloging for the local-level collection as well as the Michigan Electronic Library.

● Handled OCLC Worldcat interlibrary loan requests & fulfillment via ongoing communication with lending libraries.

Professional Involvement

Alaska Library Association - Anchorage Chapter
● Treasurer, 2012

Library Of Michigan
● Level VII Certification, 2008
● Level II Certification, 2013

Michigan Library Association Annual Conference 2014
● New Directors Conference Panel Member

Southwest Michigan Library Cooperative
● Represented the Dowagiac District Library, 2013-2015

Professional Development

Library Of Michigan Beginning Workshop, May 2008
Petoskey, MI
● Received training in cataloging, local history, collection management, children's literacy and reference service.

Public Library Association Intensive Library Management Training, October 2011
Nashville, TN
● Attended a five-day workshop focused on strategic planning, staff management, statistical analysis, collections and cataloging theory.

Alaska Library Association Annual Conference 2012 - Fairbanks, February 2012
Fairbanks, AK
● Attended seminars on EBSCO advanced search methods, budgeting, cataloging, database usage and marketing.

Depositions

2019 ● Fish & Richardson

Apple v. Qualcomm (IPR2018-001281, 39521-00421IP, IPR2018-01282 and 39521-00421IP2)

2019 ● Erise IP

Implicit, LLC v. Netscout Systems, Inc (Civil Action No. 2:18-cv-53-JRG)

2019 ● Perkins-Coie

Adobe Inc. v. RAH Color Technologies LLC (Cases IPR2019-00627, IPR2019-00628, IPR2019-00629 and IPR2019-00646)

2020 ● O'Melveny & Myers

Maxell, Ltd. v. Apple Inc. (Case No. 5:19-cv-00036-RWS)

2021 ● Pillsbury Winthrop Shaw Pittman LLP

Intel v. SRC (IPR2020-1449)

2022 ● Perkins-Coie

Realtek v. Future Link (IPR2021-01182)

2023 ● Fish & Richardson

Neuroderm Ltd. v. Abbvie, Inc (Case No. PGR2022-00040)

2023 ● Fish & Richardson

Nearmap US Inc. v. Pictometry International Corp. (IPR2022-00735)

2023 ● Fish & Richardson

Samsung Electronics v. MemoryWeb LLC (Case No. 39843-0136PS1)

2023 ● Pillsbury Winthrop Shaw Whitman LLP

Gravel Rating Systems v. Costco Wholesale Corp. (Civil Action No. 4:21-cv-149-ALM)

2024 ● Willkie-Farr

Netflix, Inc. v. VideoLabs. Inc. (IPR2023-00628)

Limited Case and Clientele History

Alston & Bird

- Ericsson

  v. Collision Communications (IPR2022-01233)

- Nokia

  v. Neptune Subsea, Xtera (Case No. 1:17-cv-01876)

- Universal Electronics Inc

  v. Roku Inc (IPR2022-00818)

Arnold & Porter

- Ivantis

  v. Glaukos (Case No. 8:18-cv-00620)

- Samsung

  v. Jawbone (Case No. 2:21-cv-00186)

Benesch Friedlander Coplan & Aronoff

- Voyis

  v. Cathx (Case No. 5:21-cv-00077-RWS)

Deschert LLP

- Smaxtec Animal Care

  v. ST Reproductive Technologies, LLC (IPR2024-00885)

Erise I.P.

- Apple

  v. Ericsson Inc. (IPR2022-00715)

  v. Future Link Systems (IPRs 6317804, 6622108, 6807505, and 7917680)

  v. INVT (Case No. 20-1881)

  v. Navblazer LLC (IPR2020-01253)

  v. Qualcomm (IPR2018-001281, 39521-00421IP, IPR2018-01282, 39521-00421IP2)

  v. Quest Nettech Corp (Case No. 2:19-cv-00118-JRG)

  v. Telefonaktiebolaget LM Ericsson (IPR2022-00275)

  v. Theta IP, LLC (IPR2024-00818)

- Fanduel

  v. CGT (Case No. 19-1393)

- Garmin

  v. Phillips North America LLC (Case No. 2:19-cv-6301-AB-KS)

- Netscout
  - v. Longhorn HD LLC (Case No. 2:20-cv-00349)
  - v. Implicit, LLC (Civil Action No. 2:18-cv-53-JRG)

- Sony Interactive Entertainment LLC
  - v. Bot M8 LLC (IPR2020-01288)
  - v. Infernal Technology LLC (Case No. 2:19-CV-00248-JRG)

- Unified Patents
  - v. GE Video Compression (Civil Action No. 2:19-cv-248)

Fish & Richardson

- Apple
  - v. AliveCor (3:21-cv-03958)
  - v. LBS Innovations (Case No. 2:19-cv-00119-JRG-RSP)
  - v. Koss Corporation (IPR2021-00305)
  - v. Masimo (IPR 50095-0012IP1, 50095-0012IP2, 50095-0013IP1, 50095-0013IP2, 50095-0006IP1, 50095-0135IP1)
  - v. Neonode (Case No. 21-cv-08872-EMC)
  - v. Qualcomm (IPR2018-001281, 39521-00421IP, IPR2018-01282, 39521-00421IP2)

- Dell
  - v. Neo Wireless (IPR2022-00616)

- Dish Network
  - v. Entropic Communications, LLC (Case No. 2:2023-CV-01043)

v. Realtime Adaptive Streaming (Case No. 1:17-CV-02097-RBJ)

v. TQ Delta LLC (Case No. 18-1798)

- Evapco Dry Cooling

  v. SPG Dry Cooling (IPR2021-00688)

- Genetec

  v. Sensormatic Electronics (Case No. 1:20-CV-00760)

- Huawei

  v. Bell Northern Research LLC (IPR2019-01174)

- Kianxis

  v. Blue Yonder (Case No. 3:20-cv-03636)

- LG Electronics

  v. Bell Northern Research LLC (Case No. 3:18-cv-2864-CAB-BLM)

- Metaswitch

  v. Sonus Networks (IPR2018-01719)

- Microsoft

  v. Throughputer Inc (IPR2022-00757)

- Mom Enterprises

  v. Ddrops Company (Case No. 1:22-cv-00332)

- MLC Intellectual Property

v. MicronTech (Case No. 3:14-cv-03657-SI)

- Nearmap Inc

  v. EagleView Technologies (IPR2022-01009)

- Neuroderm Ltd.

  v. Abbvie, Inc (Case No. PGR2022-00040)

- Realtek Semiconductor

  v. Future Link (IPR2021-01182)

- Quectel

  v. Koninklijke Philips (Case No. 1:20-cv-01710)

- Samsung

  v. Aire Technology (IPR2022-00877)

  v. Bell Northern Research (Case No. 2:19-cv-00286-JRG)

  v. Communication Technologies Inc (IPR2022-01221)

  v. Jawbone Innovations (IPR2022-00865)

  v. MemoryWeb LLC (IPR2022-00885)

  v. Dodots Licensing Solutions (IPR2023-00701)

  v. Telefonaktiebolaget LM Ericsson (IPR2021-00615)

- Texas Instruments

  v. Vantage Micro LLC (IPR2020-01261)

- Xilinx

  v. Sentient Sensors LCC (Case No. 1:22-cv-00173)

Groombridge Wu

- Nearmap

  v. Eagle View Technologies Inc. and Pictometry International Corp. (Case No. 2:21-cv-00283-TS-DAO)

Irell & Manella

- Curium

O'Melveny & Myers

- Apple

  v. Maxell (Case No. 5:19-cv-00036-RWS)

- Disney Media & Entertainment Distribution LLC

  v. Digital Media Technology Holdings, LLC (Case No. 2:22-cv-01642)

- Micron Technology Inc.

  v. Besang Inc (IPR2023-00900)

- Samsung

  v. Daedalus Prime LLC (1335 Investigation)

Perkins-Coie

- Amazon

  v. Nokia (IPR2024-00847 and IPR2024-00848)

- Heru Industries

  v. The UAB Research Foundation (IPR2022-01148)

- Intel Corporation

  v. BeSang Inc. (IPR2023-00991)

  v. BitMICRO (Case No. 5:23-cv-00625)

  v. Telefonaktiebolaget L M Ericsson (IPR2024-00610)

- Realtek Semiconductor

  v. Future Link (IPR2021-01182)

- Twitter Inc

  v. VOIP-Pal.com (Case No. 3:20-cv-02397-JD)

- TCL Industries

  v. Koninklijke Philips NV (IPR2021-00495, IPR2021-00496 and IPR2021-00497)

Pillsbury Winthrop Shaw Pittman

- Intel

  v. FG SRC LLC (Case No. 6:20-cv-00315)

- Gravel Rating Systems

  v. Costco (Case No. 4:21-cv-149)
  v. Lowe's Home Centers (Case No. 4:21-cv-150)
  v. T-Mobile USA (Case No. 4:21-cv-152)
  v. Kohl's Inc. (Case No. 4:21-cv-258)
  v. Under Armor (Case No. 4:21-cv-356)

Quinn Emanuel

- ServiceNow, Inc.

  v. InQuisient, Inc. (Case No. 22-900-CJB)

- Wolfspeed

  v. The Trustees of Purdue University (Case No. 1:2021-cv-00840)

Sheppard, Mullin, Richter & Hampton LLP

- Cadence Design Systems Inc.

  v. Semiconductor Design Technologies (Case No. 3:23-cv-01001)

Stern, Kessler, Goldstein & Fox

- Preliminary Research

Willkie, Farr & Gallagher LLP

- Neurent

  v. The Foundry, LLC (IPR2024-00669)

- Netflix, Inc.

  v. VideoLabs, Inc. (IPR2023-00628)

APPENDIX CIDRONALI01

IEEE.org | IEEE Xplore | IEEE SA | IEEE Spectrum | More Sites Subscribe Donate | Cart | Create Account | Personal Sign In

IEEE Xplore® Browse My Settings Help Institutional Sign In IEEE

All

ADVANCED SEARCH

A new approach for concurrent Dual-Band IF Digital PreDistortion: System design and analysis

Publisher: IEEE Cite This PDF

A. Cidronali ; I. Magrini ; R. Fagotti ; G. Manes **All Authors**

25 Cites in Papers | 20 Cites in Patents | 749 Full Text Views

Abstract

Document Sections

I. Introduction

II. Dual-Band Power Amplifier Architectures

III. Subsampling Receiver

IV. Dual Band Digital Predistortion

V. Simulation Results

Show Full Outline

Authors

Figures

References

Citations

Keywords

Metrics

Abstract:
In this paper we propose a dual band digital predistorter (DB-DPD), suitable for concurrent dual-band power amplifiers. A sub-sampling receiver is at the basis of the feedback path, while the vectorial gain adjuster is achieved at the proper digital intermediate frequency. The proposed method adopts a conventional memory polynomial DPD for linearization. The approach is tested by system-level simulations and it was proven to be able to correct most of the nonlinearity, with only a modest performance loss with respect to single-band architectures.

Published in: 2008 Workshop on Integrated Nonlinear Microwave and Millimetre-Wave Circuits

Date of Conference: 24-25 November 2008

DOI: 10.1109/INMMIC.2008.4745733

Publisher: IEEE

Date Added to IEEE *Xplore*: 09 January 2009

Conference Location: Malaga, Spain

ISBN Information:

I. Introduction

The most of the available Digital PreDistortion (DPD) techniques deal with single-band operation, although recently an approach to deal with multi-carrier and potentially available for multiband systems was presented in [1]. In this [illegible] width in several bands and then a DP algorithm is applied selectively [illegible] -order intermodulation distortion (IMD3). As the approach relies on third order Volterra model, the accuracy of the DP

Sign in to Continue Reading

Authors

Figures

References

Citations

Keywords

More Like This

Concurrent dual-band digital predistortion for power amplifier based on orthogonal polynomials
2013 IEEE MTT-S International Microwave Symposium Digest (MTT)
Published: 2013

Spectra-Folding Feedback Architecture for Concurrent Dual-Band Power Amplifier Predistortion
IEEE Transactions on Microwave Theory and Techniques
Published: 2015

Show More

Metrics

Usage

Select a Year

2025

View as

Graph | Table

Total usage since Jan 2011: **749**

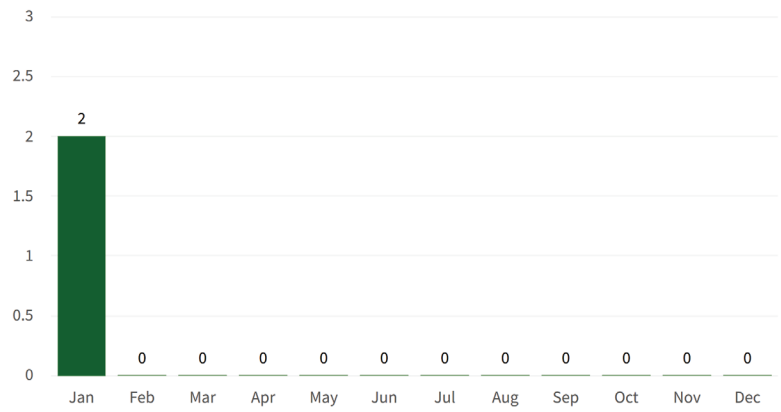

Year Total: 2
Data is updated monthly. Usage includes PDF downloads and HTML views.

Citations

Crossref® 25

Scopus® 25

Search for Citations in Google Scholar®

IEEE Personal Account

CHANGE USERNAME/PASSWORD

Purchase Details

PAYMENT OPTIONS

VIEW PURCHASED DOCUMENTS

Profile Information

COMMUNICATIONS PREFERENCES

PROFESSION AND EDUCATION

TECHNICAL INTERESTS

Need Help?

US & CANADA: +1 800 678 4333

WORLDWIDE: +1 732 981 0060

CONTACT & SUPPORT

Follow

About IEEE *Xplore* | Contact Us | Help | Accessibility | Terms of Use | Nondiscrimination Policy | IEEE Ethics Reporting | Sitemap | IEEE Privacy Policy

A public charity, IEEE is the world's largest technical professional organization dedicated to advancing technology for the benefit of humanity.

© Copyright 2025 IEEE - All rights reserved, including rights for text and data mining and training of artificial intelligence and similar technologies.

A New Approach for Concurrent Dual-Band IF Digital PreDistortion: System Design and Analysis

A. Cidronali, I. Magrini, R. Fagotti, G. Manes

Department of Electronics and Telecommunications, University of Florence, V. S. Marta, 3, I-50139, Italy {first.last@unifi.it}

***Abstract* — In this paper we propose a Dual Band Digital Predistorter (DB-DPD), suitable for concurrent dual-band power amplifiers. A sub-sampling receiver is at the basis of the feedback path, while the vectorial gain adjuster is achieved at the proper digital intermediate frequency. The proposed method adopts a conventional memory polynomial DPD for linearization. The approach is tested by system-level simulations and it was proven to be able to correct most of the nonlinearity, with only a modest performance loss with respect to single-band architectures.**

I. Introduction

The most of the available Digital PreDistortion (DPD) techniques deal with single-band operation, although recently an approach to deal with multi-carrier and potentially available for multiband systems was presented in [1]. In this technique the modulation bandwidth in several bands and then a DP algorithm is applied selectively to the inband and interband third-order intermodulation distortion (IMD3). As the approach relies on third order Volterra model, the accuracy of the DP depends upon the identification procedure and the frequency band spacing.

In this paper we propose a novel method of Dual Band DPD (DB-DPD), capable of a simultaneous predistortion of a concurrent dual-band power amplifier at both frequency bands. The proposed method uses a single band memory polynomial DP for linearization, operating at a proper IF. As feedback path the system adopts a subsampling receiver, which allows extreme flexibility and coherent dual-band down-conversion. With the selection of an appropriate sample rate, the RF channels are translated side-by-side at a low IF with no spectral overlap. At this section of the system a low-pass ADC digitizes the entire baseband range, and after DSP channelization of the signals an indirect learning algorithm is adopted to train the DPD. The memory polynomial DB-DPD system was simulated with Matlab-Simulink®, and performance was compared with those achieved from the same system operating in single band operation.

The paper is organized as follows: in Section II is recalled a brief review of the main PA topologies target of the linearization procedure herein analysed. In Section III is described the sub-sampling receiver design and the technique for the sampling frequency calculation. Section IV reports the operating principle of the DB-DP system, while in Section V simulation results are showed, highlighting performance differences over single band DPD systems.

II. Dual-band power amplifier architectures

The main objective of the present paper is the evaluation of a new concept of DB-DPD consistent with two possible architectures of dual-band PA both suitable for their involvement in the concurrent dual-band systems. The first is based on two dedicated PAs combined by a diplexer while the second is specifically designed to be operated in dual-band state. In the next paragraphs a brief discussion of this PA topologies is given.

A) Combined dedicated PAs

One out of the two dual-band architectures considered in this work is based on the schematic representation reported in Fig. 1. It represents the most straightforward solution which makes use of two dedicated PAs combined by a diplexer. While for the PA units the designer can access to the most mature and advances design methodologies and technologies, the passive diplexer still represents a very critical part of the entire PA structure. Indeed, this component must guarantee an almost lossless behavior in the transmission paths and an as much as possible isolation. In particular the former feature is required to preserve the combined efficiency of the entire structure, while the latter is a required feature to avoid the cross-modulation between the two dedicated PAs. The constraints on the diplexer become more critical in the case of closer operative spectrum bands. During the two dedicated PAs design, the eventual combination with the diplexer doesn't require specific additional PA design consideration, only an accurate evaluation of the out-of band termination which might degrade the output power and efficiency of the two units.

B) Dual-band single PA

The PA architecture under investigation in this paper is represented by the dual-band single PA, i.e. a circuit designed around a single active device and able to simultaneously operate at two different frequency bands. The schematic of the concurrent PA is reported in Fig. 2, where the dual-tuned matching networks are synthesized by either passive and\or distributed elements properly dimensioned, without external tuning controls. The basic principle discussed in [5]-[6], for the development of dual-tuned matching network can be effectively considered for the concurrent dual-band PA. In this configuration the two signal sources are combined prior to be

978-1-4244-2646-1/08/$25.00 ©2008 IEEE
Authorized licensed use limited to: June Munford. Downloaded on February 05,2025 at 19:34:40 UTC from IEEE Xplore. Restrictions apply.

Exhibit 1007
Nokia of America Corporation, et al. v. Smart RF Inc.
000029

applied to the PA input. The design method of concurrent dual-band PA based on multi-tuned networks composed of lumped elements is discussed in detail in [7].

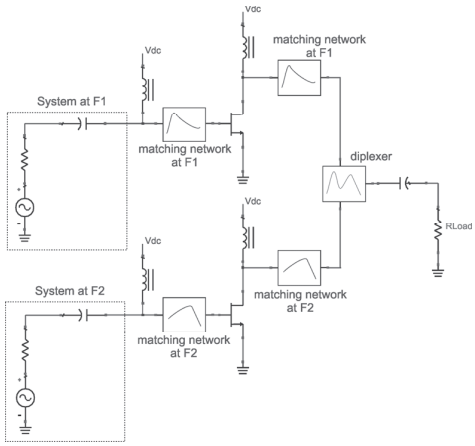

Fig. 1. Schematic of the concurrent dual-band PA implemented by two combined dedicated PAs.

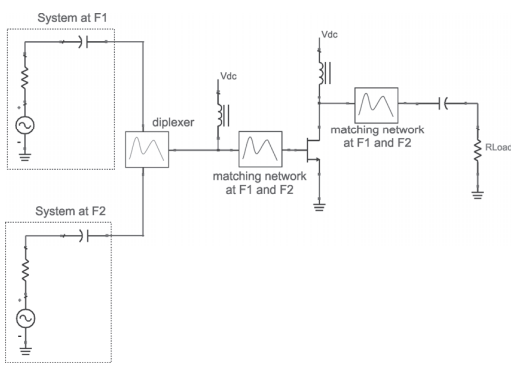

Fig. 2. Concurrent dual-band PA schematic, implemented by a dual-band PA.

III. Subsampling Receiver

The subsampling adopted in the DB-DPD feedback recalls somehow the receivers adopted in the multiband radios and is based on the bandpass sampling theorem. This principle can be adapted to down-convert two (or more) band-limited signals s_1 and s_2, located at different centre frequencies f_{c1} and f_{c2}, with bandwidths B_1 and B_2. Selecting the proper sampling frequency there will be aliases of the two signals located side-by-side in the first Nyquist zone with no overlap, as shown in Fig. 3. The sampling frequency must respect the condition:

$$f_s \geq 2(B_1 + B_2)$$

that is, the Nyquist zone must be wider than the sum of the two bands.

Form the Fig. 3 is evident that the two band-pass signals have to be down-converted at IF rather than both at base-band to make them suitable for the DP training. In the full paper a detailed discussion about the constraints and the proper selection of the intermediate frequency for the down conversions is given.

IV. Dual Band Digital PreDistortion

In the full paper we will discuss about the proposed DB-DPD system which is an extension of a single band DPD (SB-DPD) system. In this case, the predistortion is usually realized in the digital baseband, while a baseband predistortion with a unique DP is not possible in dual band concurrent systems. In DB-DP, baseband digital signals $x_1(n)$ and $x_2(n)$ are shifted to f_{IF1} and f_{IF2} then summed thus creating $\tilde{x}'(n)$, which is about a proper IF and passed through the gain adjuster; the output of this process is the numeric signal $\tilde{z}'(n)$. The next step is operated by a numeric diplexer which separates again the two frequency bands. A pair of numeric frequency down-conversions translates to baseband the two signal which are then converted in the analogue domain. This latter numeric process is required when the ADC clock frequency is an issue. The analogue PA input $\tilde{z}'(t)$ is obtained by frequency shifting to the RF frequencies f_{c1} and f_{c2}, and combining them. The PA output $\tilde{y}'(t)$, is spilled and a portion of it is used to create the feedback signals. The feedback path proposed in this paper consists of the coherent dual-band subsampling receiver discussed in the previous section. The two bands composing $\tilde{y}'(t)$ are aliased side-by-side in the baseband, then digitized by a single ADC.

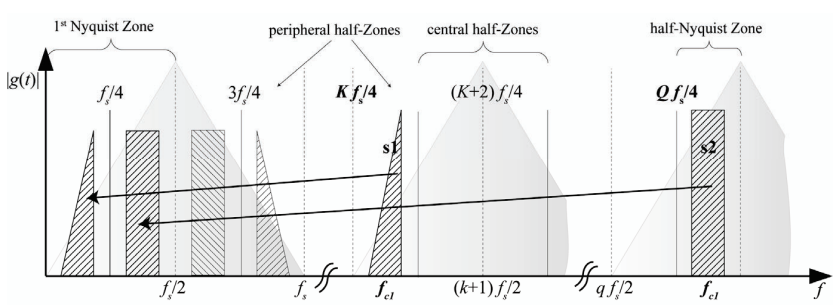

Fig. 3. Dual band subsampling

Authorized licensed use limited to: June Munford. Downloaded on February 05,2025 at 19:34:40 UTC from IEEE Xplore. Restrictions apply.

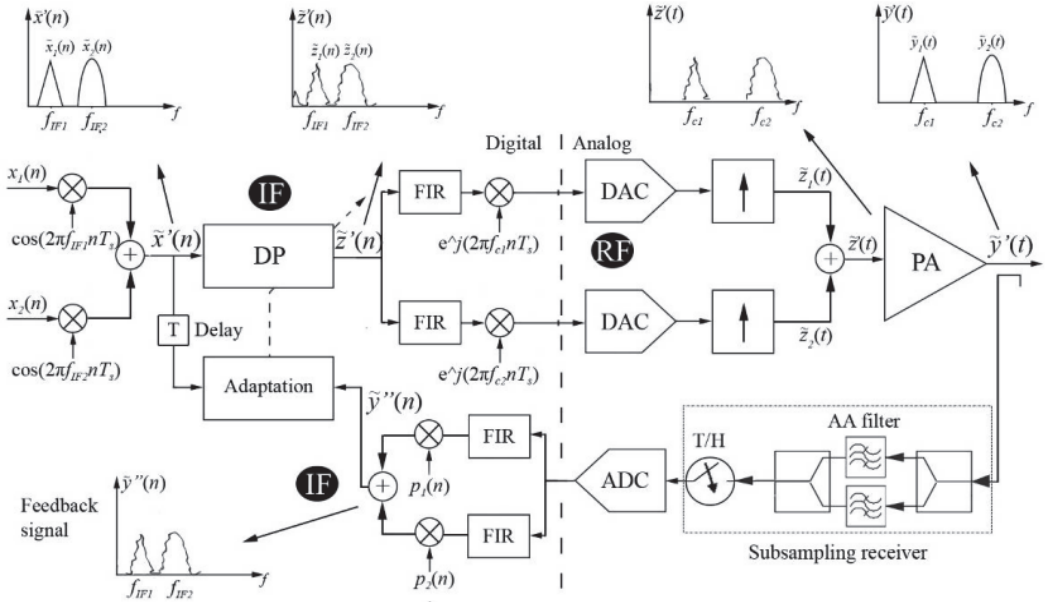

Fig. 4.DB-DP system with IF predistortion and subsampling feedback

In the digital domain, the bands are separated and shifted to IF, composing the signal $\tilde{y}''(n)$ that is compared to $\tilde{x}'(n)$ by the direct learning training algorithm. The block diagram of the whole system is shown in Fig. 4.

V. Simulation Results

The DB-DP was simulated by Matlab/Simulink®. We considered two 16 QAM signals, with amplitudes $P = -10\text{dBm}$ and centre frequencies $f_{c1} = 2.1$ GHz and $f_{c2} = 3.5$ GHz; the sampling frequency was set to $f_s = 146.5$ MHz. The PA was modeled with the Wiener-Hammerstein model. LTI blocks preceeding and following the memoryless NL were set to have the following transfer functions:

$$H(z) = \frac{1 + 0.5z^{-2}}{1 - 0.4z^{-1}} \ , \ G(z) = \frac{1 - 0.3z^{-2}}{1 - 0.4z^{-1}}$$

It was chosen a tanh-shaped AM/AM NL, that has G=20dB, IP3=38dB and whose AM/PM is linear, with 5°/dB slope.

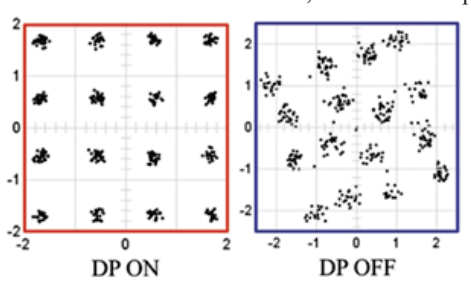

Fig. 5. Constellations comparison for lower channel, between transmitted signal and input signal, with DB-DP OFF and DB-DP ON.

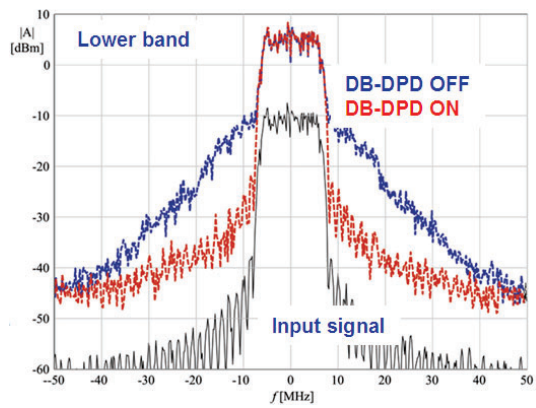

Fig. 6. Spectra comparison for lower channel, between transmitted signal and input signal, with DB-DP OFF and DB-DP ON.

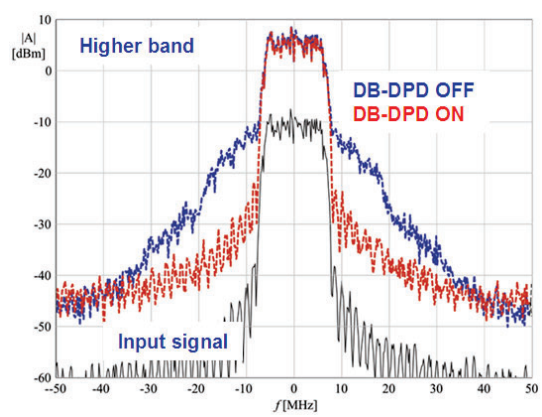

Fig. 7. Spectra comparison for higher channel, between transmitted signal and input signal, with DB-DP OFF and DB-DP ON.

Authorized licensed use limited to: June Munford. Downloaded on February 05,2025 at 19:34:40 UTC from IEEE Xplore. Restrictions apply.

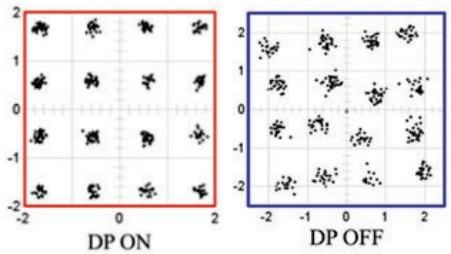

Fig. 8. Constellations comparison for higher channel, between transmitted signal and input signal, with DB-DP OFF and DB-DP ON.

For the implementation of the DB-DPD we used a memory polynomial DP, with a memory length of 4 taps, a polynomial order K=9 and a LUT predistorter with a size of 512. Polynomial coefficients were estimated on a basis of 8192 samples. Simulation results for both channels are shown in **Errore. L'origine riferimento non è stata trovata.** through **Errore. L'origine riferimento non è stata trovata.**, where an ACPR and EVM significant reduction is observed. The method proved to be able to correct most NLs, but it is not as good as a SB-DP. While in that case we obtained a Normalized Mean Square Error (NMSE) of approximately 3e-4, in the DB-DP we obtained an NMSE of approximately 1e-3.

VI. Conclusion

The proposed DB-DPD system architecture exploits a memory polynomial predistorter and a subsampling receiver as a feedback path. The DB-DP implements a memory polynomial predistorter and a direct learning training method similar to those involved in single band DP. It operates at a proper digital IF and it is able to correct most NLs, even those due to memory effect, both in single and dual band operation. The introduced technique can be effectively used in conjunction with concurrent dual-band PAs. Comparison with conventional DPD shows that the performance decreases slightly when a concurrent dual band signal is predistorted.

References

[1] P. Roblin, S. K. Myoung, D. Chaillot, Y. Gi Kim, A. Fathimulla, J. Strahler, S. Bibyk ”Frequency-Selective Predistortion Linearization of RF Power Amplifiers” IEEE Trans on Microwave Theory and Tech., Vol. 56, Jan. 2008, pp 65-76

[2] L. Ding, GT Zhou, DR Morgan, Z. Ma, JS Kenney, J. Kim, and CR Giardina. Memory polynomial predistorter based on the indirect learning architecture. *Global Telecommunications Conference, 2002. GLOBECOM'02. IEEE, 1, 2002.*

[3] R. Meyer, R. Eschenback, and W. Edgerley, Jr., “A wideband feedforward amplifier,” *IEEE J. Solid-State Circuits*, vol. SCC-9, no. 6, pp. 422–448, Jun. 1974.

[4] Y. Kunisawa “Study on a Multiple Signal Receiver Using Undersampling Scheme” Proc. of 2005 Software Defined Radio Technical Conference, and Product Exposition Nov. 14-18, 2005

[5] D. Bespalko, N. Messaoudi, S. Boumaiza, ‘Concurrent dual-band GaN Power Amplifier with compact micro-strip matching network’ 2008 IEEE Topical Symposium on Power Amplifier for Wireless Communications, Jan. 21-22, 2008, Orlando, Florida

[6] P. Colantonio, F. Giannini, R. Giofre, L. Piazzon, “Simultaneous dual-band high efficiency harmonic tuned power amplifier in GaN technology”, European Microwave Integrated Circuit Conference, 8-10 Oct. 2007 pp.127 – 130

[7] A. Cidronali, N. Giovannelli, I. Magrini G. Manes “Dual-band Compact Concurrent Dual-Band Power Amplifier for 1.98 GHz WCDMA and 3.42 GHz OFDM Wireless Systems: Design and Characterization”, 38th European Microwave Conference, Amsterdam Oct. 27th, 2008

Authorized licensed use limited to: June Munford. Downloaded on February 05,2025 at 19:34:40 UTC from IEEE Xplore. Restrictions apply.

APPENDIX CIDRONALI02

```
LEADER 00000cam a2200505 a 4500
001    IEEE318460434
006    m     o  d
007    cr mn|||||||||
008    090414s2008    njua    ob    101 0 eng d
020    9781424426461
020    1424426464
020    9781424426454
020    1424426456
040    STF|beng|epn|cSTF|dSTF|dIEEXO|dOCLCQ|dOCLCF|dOCLCO|dOCLCQ
       |dOCL|dOCLCO|dOCLCQ|dIAS|dCEF|dDEHBZ|dOCLCQ|dLVT|dOCLCO
       |dOCLCQ
049    RVEU
050  4 TK7871.58.P6
099    ELECTRONIC|aRESOURCES
111 2  International Workshop on Integrated Nonlinear Microwave
       and Millimeterwave Circuits|d(2008 :|cUniversidad de
       Málaga)
245 10 INMMIC Málaga :|bInternational Workshop on Integrated
       Nonlinear Microwave and Millimeterwave Circuits 2008 :
       2425 November 2008, E.T.S. Ingeniería de Telecomuncación,
       Universidad de Málaga, Málaga, Spain : proceedings
246 1  |iAvailable from some providers with title:|aIntegrated
       Nonlinear Microwave and MillimetrWave Circuits, 2008,
       NMMIC 2008, Workshop on
246 3  Workshop on Integrated Nonlinear Microwave and
       MillimetrWave Circuits, 2008
260    [Piscataway, N.J.] :|bIEEE,|c©2008
264  4 |c©2008
300    1 online resource ([180] pages) :|billustrations
336    text|btxt|2rdacontent
337    computer|bc|2rdamedia
338    online resource|bcr|2rdacarrier
490 0  Proceedings of the IEEE
490 0  IEEE Xplore All Conference Proceedings
500    Title from PDF cover (viewed Apr 14, 2009)
500    "IEEE Catalog Number: CFP0894A."
504    Includes bibliographical references and index
506    Access is limited to RIT students, faculty and staff
538    MODE OF ACCESS: World Wide Web
590    Subsequent record output
650  0 Power amplifiers|vCongresses
650  0 Microwave integrated circuits|vCongresses
650  0 Millimeter wave devices|vCongresses
655  7 Electronic books.|2local
776 08 |iPrint version:|aInternational Workshop on Integrated
       Nonlinear Microwave and Millimeterwave Circuits (2008 :
       Universidad de Málaga).|tINMMIC Málaga.|d[Piscataway,
       N.J.] : IEEE, ©2008|w(DLC)  2008905036
856 40 |zIEEE Electronic Books|uhttps://ezproxy.rit.edu/
       login?url=https://ieeexplore.ieee.org/servlet/
       opac?punumber=4740201
```

RIT | Libraries

Hours | Chat | My Library Acco

Start Over | Save Records | MARC Display | Another Search

ISSN/ISBN | 978-1-4244-2646-1 | Entire Catalog | System Sorted | Search

Limit search to available items

Previous Record Next Record

Author International Workshop on Integrated Nonlinear Microwave and Millimeterwave Circuits (2008 : Universidad de Málaga)

Title **INMMIC Málaga : International Workshop on Integrated Nonlinear Microwave and Millimeterwave Circuits 2008 : 2425 November 2008, E.T.S. Ingeniería de Telecomuncación, Universidad de Málaga, Málaga, Spain : proceedings**

Publisher [Piscataway, N.J.] : IEEE, ©2008
©2008

Available electronically:

IEEE Electronic Books

Permanent Link

ISSN/ISBN 9781424426461
1424426464
9781424426454
1424426456

Descript 1 online resource ([180] pages) : illustrations

Content text

Media computer

Carrier online resource

Call No. TK7871.58.P6

Series Proceedings of the IEEE
IEEE Xplore All Conference Proceedings

Notes Includes bibliographical references and index
Title from PDF cover (viewed Apr 14, 2009)
"IEEE Catalog Number: CFP0894A."
Access is limited to RIT students, faculty and staff
MODE OF ACCESS: World Wide Web
Subsequent record output

Subject Power amplifiers -- Congresses
Microwave integrated circuits -- Congresses
Millimeter wave devices -- Congresses
Electronic books. local

Alt Title Available from some providers with title: Integrated Nonlinear Microwave and MillimetrWave Circuits, 2008, NMMIC 2008, Workshop on
Workshop on Integrated Nonlinear Microwave and MillimetrWave Circuits, 2008

Contact Us | InterLibrary Loan

APPENDIX CIDRONALI03

```
leader  02794cam  2200625Ia 4500
001     990017069080106761
005     20241128031711.0
006     m        d
007     cr mn|
008     090414s2008    njua    sb    101 0 eng d
010     ##$z  2008905036
020     ##$a9781424426461
020     ##$a1424426464
020     ##$a9781424426454
020     ##$a1424426456
035     ##$a(MCM)001706908MIT01
035     ##$a(OCoLC)318460434
040     ##$aSTF $cSTF $dSTF $dIEEXO $dMYG
049     ##$aMYGG
050     #4$aTK7871.58.P6
111     2#$aInternational Workshop on Integrated Nonlinear Microwave and Millimeterwave Circuits $d(2008 : $cUniversidad de Málaga)
245     10$aINMMIC Málaga $h[electronic resource] : $bInternational Workshop on Integrated Nonlinear Microwave and Millimeterwave Circuits 2008 : 2425 November 2008, E.T.S. Ingeniería de Telecomuncación, Universidad de Málaga, Málaga, Spain : proceedi
246     1#$iAvailable from some providers with title: $aIntegrated Nonlinear Microwave and MillimetrWave Circuits, 2008, NMMIC 2008, Workshop on
246     13$aWorkshop on Integrated Nonlinear Microwave and MillimeterWave Circuits, 2008
260     ##$a[Piscataway, N.J.] : $bIEEE, $cc2008.
300     ##$a1 online resource ([180] p.) $bill.
336     ##$atext $btxt $2rdacontent
337     ##$acomputer $bc $2rdamedia
338     ##$aonline resource $bcr $2rdacarrier
504     ##$aIncludes bibliographical references and index.
500     ##$aTitle from PDF cover (viewed on Apr. 14, 2009).
506     ##$aAccess restricted to licensed sites/users.
538     ##$aMode of access: World Wide Web.
500     ##$a"IEEE Catalog Number: CFP0894A."
650     #0$aPower amplifiers $vCongresses.
650     #0$aMicrowave integrated circuits $vCongresses.
650     #0$aMillimeter wave devices $vCongresses.
650     #7$aMillimeter wave devices. $2fast
650     #7$aMicrowave integrated circuits. $2fast
650     #7$aPower amplifiers. $2fast
655     #7$aConference papers and proceedings. $2lcgft
655     #7$aConference papers and proceedings. $2fast
710     2#$aIEEE Xplore (Online service)
856     40$uhttp://ieeexplore.ieee.org/servlet/opac?punumber=4740201 $3IEEE Xplore
910     ##$aabf100212 $iabf $d100212
910     ##$aMARCIVEAUT
910     ##$aMARCIVEAUT221103
910     ##$aMARCIVEAUT231208
910     ##$aMARCIVEAUT241113
946     ##$mIEEE
949     #1$1MIT Access Only $an-mit $bNET $h**See URL(s) $o8 $x02
960     ##$aInternational Workshop on Integrated Nonlinear Microwave and Millimeterwave Circuits 2008 Universidad de Málaga
961     ##$a[Piscataway, N.J.] : IEEE,   $a 2008  $a nju
969     ##$aTK7871.58.P6 $a318460434 $a9781424426461 $a1424426464 $a9781424426454 $a1424426456
994     ##$a02 $bMYG
```

Ask Us Chat

CONFERENCE PROCEEDING

INMMIC Málaga International Workshop on Integrated Nonlinear Microwave and Millimeterwave Circuits 2008 : 2425 November 2008, E.T.S. Ingeniería de Telecomuncación, Universidad de Málaga, Málaga, Spain : proceedings.

International Workshop on Integrated Nonlinear Microwave and Millimeterwave Circuits (2008 : Universidad de Málaga); IEEE Xplore (Online service)

c2008

Available Online

Actions

PRINT CITATION EXPORT RIS EXPORT BIBTEX EXPORT TO EXCEL/CSV LINK EMAIL

Get it online

Online availability

IEEE Xplore Conference Proceedings

More options

IEEE Xplore

View record metadata - MARC format

Details

Title	INMMIC Málaga International Workshop on Integrated Nonlinear Microwave and Millimeterwave Circuits 2008 : 2425 November 2008, E.T.S. Ingeniería de Telecomuncación, Universidad de Málaga, Málaga, Spain : proceedings.
Creator	International Workshop on Integrated Nonlinear Microwave and Millimeterwave Circuits (2008 : Universidad de Málaga) IEEE Xplore (Online service)
Subject	Power amplifiers Microwave integrated circuits Millimeter wave devices
Genre	Congresses Conference papers and proceedings
Other title	Available from some providers with title: Integrated Nonlinear Microwave and MillimetrWave Circuits, 2008, NMMIC 2008, Workshop on Workshop on Integrated Nonlinear Microwave and MillimeterWave Circuits, 2008
Publisher	Piscataway, N.J. : IEEE
Creation Date	c2008
Format	1 online resource ([180] p.) ill.
Source	Library Catalog
Notes	Title from PDF cover (viewed on Apr. 14, 2009). "IEEE Catalog Number: CFP0894A." Includes bibliographical references and index.
Identifier	ISBN : 9781424426461 ISBN : 1424426464 ISBN : 9781424426454 ISBN : 1424426456 OCLC : (OCoLC)318460434

Ask Us Chat

Browse virtual shelf

IEEE
cal
erence on
licrowave
er ...

2017 IEEE Topical Conference on Power Amplifiers for ...
2017

High-efficiency load modulation power amplifiers for ...
2017

INMMIC Málaga International Workshop on Integrated ...
c2008

Microwave power amplifier design with MMIC modules ...
2018

APPENDIX CIDRONALI04

VILLANOVA UNIVERSITY VISIT / APPLY / GIVE 0 ITEMS MY LIBRARY ACCOUNT

FALVEY LIBRARY COLLECTIONS RESEARCH SERVICES USING THE LIBRARY ABOUT

Search Books & Media books, dvds, CDs, other media Advanced Search Tips

COMBINED SEARCH BOOKS & MEDIA ARTICLES & MORE

INMMIC Málaga

Cite this Text this Email this Print Export Record Save to List Add to Book Bag Permanent link

INMMIC Málaga International Workshop on Integrated ...

INMMIC MÁLAGA INTERNATIONAL WORKSHOP ON INTEGRATED NONLINEAR MICROWAVE AND MILLIMETERWAVE CIRCUITS 2008 : 2425 NOVEMBER 2008, E.T.S. INGENIERÍA DE TELECOMUNCACIÓN, UNIVERSIDAD DE MÁLAGA, MÁLAGA, SPAIN : PROCEEDINGS.

Corporate Authors:	International Workshop on Integrated Nonlinear Microwave and Millimeterwave Circuits Universidad de Málaga, IEEE XPlore Conference Proceedings Online
Format:	Online, Conference Proceeding, Book
Language:	English
Published:	[Piscataway, N.J.] : IEEE, c2008.
Subjects:	Microwave integrated circuits > Congresses. Millimeter wave devices > Congresses. Power amplifiers > Congresses.
Access:	Online version
Tags:	No Tags, Be the first to tag this record! Add Tag

Holdings Description Comments Similar Items Staff View

MARC

LEADER			00000cam a2200000Ia 4500
001			1450511
005			20130708111525.0
006			m d
007			cr mn|
008			090414s2008 njua ob 101 0 eng d
020			**|a** 1424426456
020			**|a** 1424426464
020			**|a** 9781424426454
020			**|a** 9781424426461
035			**|a** (OCoLC)318460434
035			**|a** (OCoLC)ocn318460434
040			**|a** STF **|b** eng **|c** STF **|d** STF **|d** IEEXO **|d** OCLCQ
049			**|a** PVUM
050		4	**|a** TK7871.58.P6
111	2		**|a** International Workshop on Integrated Nonlinear Microwave and Millimeterwave Circuits **|d** (2008 : **|c** Universidad de Málaga)
245	1	0	**|a** INMMIC Málaga **|h** [electronic resource] : **|b** International Workshop on Integrated Nonlinear

SIMILAR ITEMS

INMMiC 2006 International Workshop on Integrated Nonlinear Microwave and Millimeter-Wave Circuits : proceedings : January, 30th-31st, 2006, Universidade de Aveiro, Aveiro, Portugal.
Published: (2006)

INMMIC Göteborg 2010 Workshop on Integrated Nonlinear Microwave and Millimetre-Wave Circuits : conference proceedings : April, 26-27th, 2010, Chalmers University of Technology, Göteborg, Sweden /
Published: (2010)

2012 Workshop on Integrated Nonlinear Microwave and Millimetre-Wave Circuits INMMIC Dublin : 3rd-4th September 2012, Dublin, Ireland /
Published: (2012)

2011 Workshop on Integrated Nonlinear Microwave and Millimetre-Wave Circuits Vienna, Austria, April 18th-19th, 2011
Published: (2011)

Tutorial Colloquium on Design of RFIC's and MMIC's [proceedings], Savoy Place, London, Wednesday, 26 November 1997 /
Published: (1997)

			Microwave and Millimeterwave Circuits 2008 : 2425 November 2008, E.T.S. Ingeniería de Telecomuncación, Universidad de Málaga, Málaga, Spain : proceedings.
246	1		**|i** Available from some providers with title: **|a** Integrated Nonlinear Microwave and MillimetrWave Circuits, 2008, NMMIC 2008, Workshop on
246	3		**|a** Workshop on Integrated Nonlinear Microwave and MillimetrWave Circuits, 2008
260			**|a** [Piscataway, N.J.] : **|b** IEEE, **|c** c2008.
300			**|a** 1 online resource ([180] p.) : **|b** ill.
500			**|a** "IEEE Catalog Number: CFP0894A."
500			**|a** Title from PDF cover (viewed Apr. 14, 2009).
504			**|a** Includes bibliographical references and index.
506			**|a** Electronic access restricted to Villanova patrons.
598			**|a** 08-JUL-13
650		0	**|a** Microwave integrated circuits **|v** Congresses.
650		0	**|a** Millimeter wave devices **|v** Congresses.
650		0	**|a** Power amplifiers **|v** Congresses.
710	2		**|a** IEEE XPlore Conference Proceedings Online.
776	0	8	**|i** Print version: **|a** International Workshop on Integrated Nonlinear Microwave and Millimeterwave Circuits (2008 : Universidad de Málaga). **|t** INMMIC Málaga. **|d** [Piscataway, N.J.] : IEEE, c2008 **|w** (DLC) 2008905036
856	4	0	**|z** Online version **|u** http://ezproxy.villanova.edu/login?URL=http://ieeexplore.ieee.org/servlet/opac?punumber=4740201 **|t** 0
994			**|a** 92 **|b** PVU
999	f	f	**|i** 538693b3-8462-52b5-b27b-004d137a0280 **|s** a7425d0a-682b-58e0-acff-2c8116b9b7eb **|t** 0
952	f	f	**|p** Default **|a** Villanova University **|b** Villanova PA **|c** Falvey Memorial Library **|d** World Wide Web **|t** 0 **|e** TK7871.58.P6 **|h** Library of Congress classification **|i** Electronic Books **|n** 0

COLLECTIONS
Tools
Collection Development
Distinctive Collections
Highlighted Collections

RESEARCH SERVICES
Ask a Librarian
Guides and Tools
Teaching and Learning
Digital Research and Publishing Support

USING THE LIBRARY
Access
Spaces
Technology
Borrow and Request
Learning Commons
Services For...

ABOUT
Overview
Library Organization
Events
Visit
Contact Us
News
Library Initiatives
Give to the Library
Jobs @ Falvey

Support Our Library

VILLANOVA UNIVERSITY 800 Lancaster Ave., Villanova, PA 19085 610.519.4500 Contact

DIRECTIONS PRIVACY & SECURITY DIVERSITY HIGHER EDUCATION ACT MY NOVA DIRECTORY WORK AT VILLANOVA ACCESSIBILITY

Back to Top Ask Us: Live Chat

APPENDIX CIDRONALI05

Google Scholar

SIGN IN

Articles

1 result (**0.01** sec)

My profile My library

Any time
Since 2025
Since 2024
Since 2021
Custom range...
2009 — 2010
Search

Sort by relevance
Sort by date

Create alert

A new approach for concurrent dual-band IF digital predistortion: System design and analysis

Search within citing articles

Flexible Power Amplifier Architectures for Spectrum Efficient Wireless Applications

[PDF] researchgate.net

A Cidronali, I Magrini, G Manes - Advanced Microwave Circuits …, 2010 - books.google.com

The wireless systems evolution known as "beyond the 3rd generation"(B3G) will make use of dynamic spectrum access techniques to provide wide bandwidth to mobile users via …

Save Cite Related articles All 5 versions

Scholar PDF Reader Try now No thanks

Follow references Skim outline Cite and save

Privacy Terms Help

APPENDIX CIDRONALI06

OPEN ACCESS

Flexible Power Amplifier Architectures for Spectrum Efficient Wireless Applications

WRITTEN BY

Alessandro Cidronali, Iacopo Magrini and Gianfranco Manes

Published: 01 April 2010

DOI: 10.5772/8426

CHAPTER METRICS OVERVIEW

3,484 Chapter Downloads

View Full Metrics

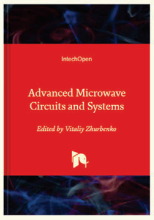

FROM THE EDITED VOLUME

Advanced Microwave Circuits and Systems

Edited by Vitaliy Zhurbenko

Book Details | Order Print

REGISTER TO DOWNLOAD FOR FREE

Share Cite

ADVERTISEMENT

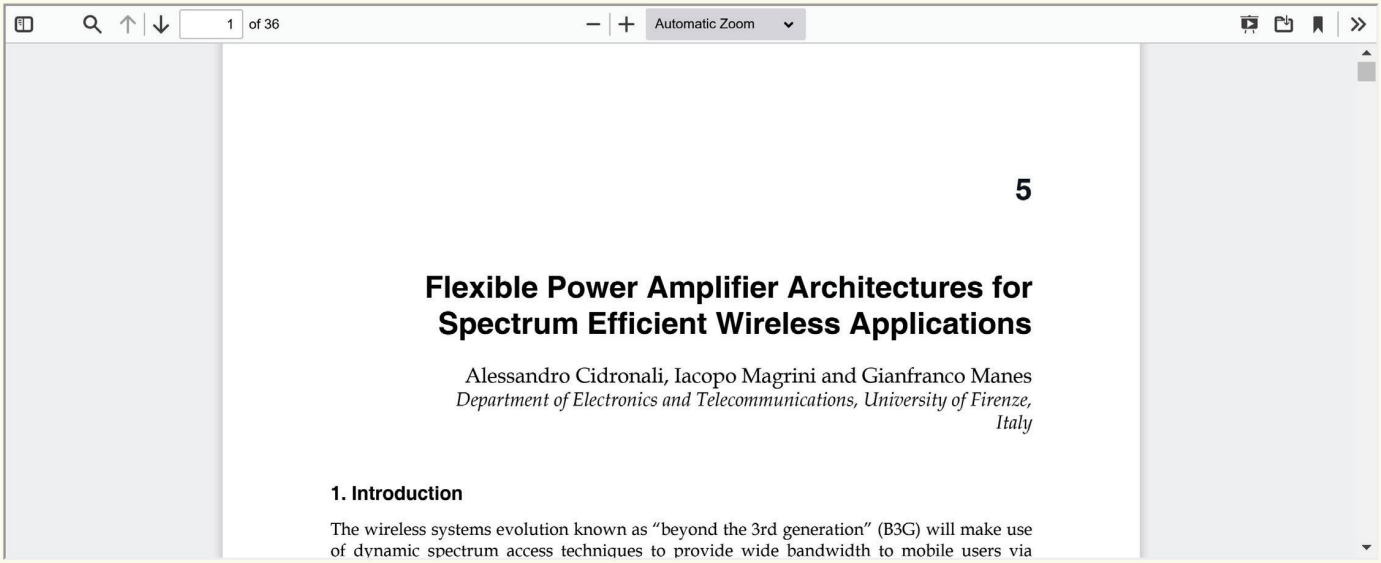

5

Flexible Power Amplifier Architectures for Spectrum Efficient Wireless Applications

Alessandro Cidronali, Iacopo Magrini and Gianfranco Manes
Department of Electronics and Telecommunications, University of Firenze, Italy

1. Introduction

The wireless systems evolution known as "beyond the 3rd generation" (B3G) will make use of dynamic spectrum access techniques to provide wide bandwidth to mobile users via

WRITTEN BY

Alessandro Cidronali, Iacopo Magrini and Gianfranco Manes

Published: 01 April 2010

REGISTER TO DOWNLOAD FOR FREE Share Cite

© 2010 The Author(s). Licensee IntechOpen. This chapter is distributed under the terms of the Creative Commons Attribution-NonCommercial-ShareAlike-3.0 License, which permits use, distribution and reproduction for non-commercial purposes, provided the original is properly cited and derivative works building on this content are distributed under the same license.

CONTINUE READING FROM THE SAME BOOK

View All

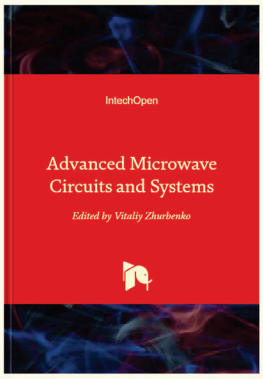

Advanced Microwave Circuits and Systems

Edited by Vitaliy Zhurbenko

PUBLISHED: 01 APRIL 2010

CHAPTER 1

Mixed-Mode S-Parameters and Conversion Techniques

By Allan Huynh, Magnus Karlsson and Shaofang Gong

15333 DOWNLOADS

CHAPTER 2

A Thru-Only De-Embedding Method Foron-Wafer Charac...

By Shuhei Amakawa, Noboru Ishihara and Kazuya Masu

7974 DOWNLOADS

CHAPTER 3

Current reuse topology in UWB CMOS LNA

By Taris Thierry

5257 DOWNLOADS

Home
News
Contact
Careers
SDG Hub

About
Authors, Editors and Institutions
Scientific Advisors
Team
Events
Advertising
Memberships and Partnerships

Publish
About Open Access
How it Works
OA Publishing Fees
Open Access Funding
Peer Review
Editorial Policies

IntechOpen Limited
167-169 Great Portland Street,
London, W1W 5PF,
UNITED KINGDOM

Phone: +44 20 8089 5702

Search

AUTHOR PANEL SIGN IN

© 2025 IntechOpen. All rights reserved.

Terms and Conditions | Privacy Policy | Customer Complaints

We are IntechOpen, the world's leading publisher of Open Access books
Built by scientists, for scientists

7,400
Open access books available

194,000
International authors and editors

210M
Downloads

Our authors are among the

154
Countries delivered to

TOP 1%
most cited scientists

14%
Contributors from top 500 universities

CLARIVATE ANALYTICS
BOOK CITATION INDEX
INDEXED

WEB OF SCIENCE™

Selection of our books indexed in the Book Citation Index in Web of Science™ Core Collection (BKCI)

Interested in publishing with us?
Contact book.department@intechopen.com

Numbers displayed above are based on latest data collected.
For more information visit www.intechopen.com

5

Flexible Power Amplifier Architectures for Spectrum Efficient Wireless Applications

Alessandro Cidronali, Iacopo Magrini and Gianfranco Manes
Department of Electronics and Telecommunications, University of Firenze, Italy

1. Introduction

The wireless systems evolution known as "beyond the 3rd generation" (B3G) will make use of dynamic spectrum access techniques to provide wide bandwidth to mobile users via heterogeneous wireless networks. A consistent step toward this scenario is represented by the outcome of the last World Radiocommunication Conference [1] which established new primary frequency bands allocation spanning from the UHF band to low microwaves and thus reflecting the increasing demands for broadband mobile and cellular systems.
We have become used to the doubling of processing power of chips based on Moore's law, but the progress in radio interface technologies still poses significant challenges.
High spectrum efficiency performance becomes therefore another major requirement of the design, along with the more consolidated ones: energy efficiency, integration, cost and reliability.
While the IMT-advanced roadmap foresees a 100 Mbps data rate for mobile users and a peak of 1 Gbps is expected for nomadic users, the available spectrum for legacy wireless communications is fragmented and reaches the amount of 750 MHz in the S-C band. A radio technology that is expected to interact with a multi-services network should be able to change between different operating bands and adapt its features according with the different available standard and requirements. Most of the research efforts performed during the last years dealt with issues related to the physical layer of the communication stack [2]; however, despite the growing interest in multi-standard operation, less attention has been devoted to the radio-frequency front-end, which therefore remains one of the most challenging parts of a multi-band radio. One main reason for the delay in effectively implementing multi-standard transceivers can be attributed to the implementation of the RF transmit power amplifier (PA). Today, dedicated, single standard PAs achieve very good power added efficiency (PAE) and, in this way, long battery lifetime. Any multi-standard PA, needed for the support of different, not always predefined, communication systems, should compete with such dedicated solutions. A conceptual framework to this is provided by the so-called software-defined radio (SDR), i.e. a radio communication system, using software for the reconfiguration of the digital and analog parts in order to perform the modulation and demodulation of radio signals, [3]. In practice, however, due to the difficulty of implementing the fast signal processing implied in the SDR approach, most of

Exhibit 1007
Nokia of America Corporation, et al. v. Smart RF Inc.
000050

the systems on the market, based on more traditional approaches, are still supporting only a very limited number of standards (e.g. 4 GSM frequencies, UMTS and, possibly, Bluetooth). In the near future, further standards will have to be supported, and more could have to be added during the handset lifetime, hopefully without hardware reconfiguration. This will determine the need of multiband PAs capable to transmit efficiently more than one service with variable radio access schemes.

Example of realizations in different technologies are provided in this Chapter as demonstrators of the discussed multiband design methods. The flexibility of the operative frequency is thus introduced by analyzing new PA architectures and design methodologies which consider the inclusion of tunable and switching components to enable a change in the operative frequency. A review of the most promising circuit topologies suitable to design reconfigurable matching networks is given in this Chapter. Varactor diodes based and MOS switched based topologies are compared, highlighting their point of strength and weakness. It is shown as a concurrent dual-band PA implemented by the proper combination of frequency-dedicated PAs, each of them optimized to work in a given bandwidth would be an easy approach, it becomes unsuited due to the complexity of the power combiners. For this reason the true concurrent dual band PA presented in this chapter is to be considered as an enabler components for high efficiency multiband systems.

Spectrum efficiency is just one of the challenges a wireless system designer faces, further come from linearity and energy efficiency resulting from the use of multicarrier and complex envelope modulation schemes. As the spectrum efficiency increases a more demanding requirement in term of PA linearity faces to the designers. Energy efficiency and linearity are conventionally traded-off considering that increasing the power back-off increases the linearity at the expenses of lower energy efficiency. To maintain signal integrity, the resulting waveforms in turn require linear transmission paths for their successful deployment. A way to match signal integrity and energy efficiency consists in the use of digital predistortion algorithm applied at base-band and implemented in the digital section of the transmitter. In spite of their large development in frequency dedicated PA architectures, the development of a technique suitable for multi-band applications is not yet completely available. In this Chapter a comprehensive treatment a novel technique for Dual Band Digital Predistortion (DB-DP) is discussed. The DB-PD is based on the simultaneous predistortion of both channels at intermediate frequency (IF), it uses a single band memory polynomial DP for linearization, while the feedback path is based on a subsampling receiver. The memory polynomial DB-DP system is presented by simulation with Matlab-Simulink® for a deep understanding of performance.

2. A possible applicative scenario for multi-band transmitters

Extending the scenario to already experienced 3G voice/data systems, users may be moving while simultaneously operating in a broadband data access or multimedia streaming session. The need to support low latency and low packet loss handovers of data streams as users transition from one access point to another may require the concurrent use of more than one frequency band at the time. For full-mobile data services, no user interaction will be required to adapt their service expectations because of environmental limitations that are technically challenging but not directly relevant to the user (such as being stationary or moving). The enabling front-end of future mobile unit thus will accommodate more than

Exhibit 1007
Nokia of America Corporation, et al. v. Smart RF Inc.
000051

one system in a effective and efficient way to make possible the connectivity capabilities depicted in Fig. 1.

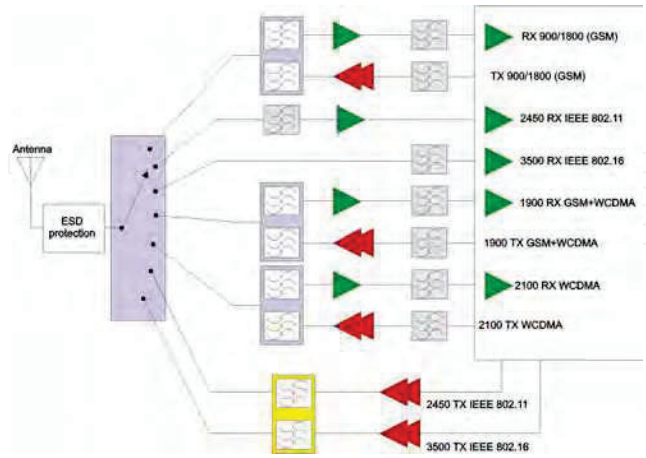

Fig. 1. Concept of a multi-band transmitter

The Wireless Local Area Network (WLAN) industry has become one of the fastest growing segments of the communications industry. This growth is due, in large part, to the introduction of standards-based WLAN products, regulated by the IEEE 802.11. The expectation of the WLAN's continuing growth stems from the promise of new standardized WLAN technologies, from improved cost/performance of WLAN systems, and from the growing availability of WLAN solutions that consolidate voice, data, and mobility functions. This, combined with market forecasts reporting that WLAN will experience a continuous growth in the next years, show that WLAN technologies will play a significant role in the future and will have a significant impact on our business and personal life styles. The WiMAX is an alternative and complementing standard for high data rate transmission, which will transform the world of mobile broadband by enabling the cost-effective deployment of metropolitan area networks based on the IEEE 802.16 standard to support notebook PC and mobile users on move. There are many advantages of systems based on 802.16, e.g. the ability to provide service even in areas that are difficult for wired infrastructure to reach and the ability to overcome the physical limitations of traditional wired infrastructure. The standard will offer wireless connectivity of up to 30 miles. The major capabilities of the standard are its widespread reach, which can be used to set up a metropolitan area network, and its data capacity of 75 Mbps. This high-speed wireless broadband technology promises to open new, economically viable market opportunities for operators, wireless Internet service providers and equipment manufacturers. The flexibility of wireless technology, combined with high throughput, scalability and long-range features of the IEEE 802.16 standard helps to fill the broadband coverage gaps and reach millions of new residential and business customers worldwide.

With WLAN 802.11 and now WiMAX 802.16, there has been a growing interest in technologies that allow delivery of higher data rates over large geographical areas. The IEEE 802.16 family of standards (802.16-2004 and 802.16e) are intended to provide high

Exhibit 1007
Nokia of America Corporation, et al. v. Smart RF Inc.
000052

bandwidth wireless voice and data for residential and enterprise use. The modulation used to achieve these high data rates is orthogonal frequency-division multiplexing (OFDM). WiMAX OFDM features a minimum of 256 subcarriers up to 2048 subcarriers, each modulated with either BPSK, QPSK, 16 QAM or 64 QAM modulation. Having these carriers orthogonal to each other minimizes self-interference. This standard also supports different signal bandwidths, from 1.25 MHz to 20 MHz to facilitate transmission over longer ranges and to accommodate different multipath environments. This represents a significant increase in system profile complexity as compared to the 802.11 standard, mostly to guarantee a wider, more efficient, more robust network. More subcarriers and variable-length guard intervals contribute to this enhancement.

The ability to develop and manufacture a single reconfigurable terminal, which can be configured at the final stage of manufacture to tailor it to a particular market, clearly presents immense benefits to equipment manufacturers. With the design, components used, and hardware manufacturing processes all being identical for all terminals worldwide, the economy of scale would be huge. This has the potential to offset the additional hardware costs which would be inevitable in the realisation of such a generic device.

Based on this, the scenario adopted reflects in the request for transceiver architectures capable to support cellular phone, WLAN and WiMAX in an 'always and everywhere connected' solution. The transceiver performance in this multi-standard operation, however, comes at the expense of RF specifications that are more difficult to achieve. Furthermore, the choice and definition of the proper transceiver architecture becomes a difficult task, since several parameters - as now imposed by two standards - must be taken into account.

3. Suitable architectures for multiband-multimode transmitters

The concept of a multiband or general coverage terminal is, strictly speaking, an extension of the basic SDR concept into that of a broadband flexible architecture radio, since the basic reconfigurability and adaptability aspects of operation do not depend upon multiband coverage. It would be possible, for example, to construct a useful SDR which operated in the 800-900 MHz area of spectrum and which could adapt between AMPS, GSM, DAMPS, PDC, and CDMA. It is now normal, however, for a handset to have multi-frequency operation and hence the extension of this principle to a SDR is a natural one. The international business traveler market is still seen as both large and lucrative, particularly in terms of call charges, hence making this type of handset attractive to both manufacturers and network providers. An ideal SDR is shown in Fig. 2; note that the A/D converter is assumed to have a built-in anti-alias filter and that the D/A is assumed to have a built-in reconstruction filter.

The ideal software defined radio has the following features [4]:

- The radio access scheme (i.e. modulation scheme, channelization, coding) and equalization for transmitter and receiver are all determined in software within the digital processing subsystem. This is shown containing a DSP in Fig. 2
- The ideal circulator is used to separate the transmit and receive path signals, without the usual frequency restrictions placed upon this function when using filter-based solutions (e.g., a conventional diplexer). This component relies on ideal matching between itself and the antenna and power amplifier impedances and so is unrealistic in practice over a broad frequency band. Since the primary

Exhibit 1007
Nokia of America Corporation, et al. v. Smart RF Inc.
000053

alternative, a diplexer, is very much a frequency-dedicated component, its elimination is a key element in a multiband or even multimode transceiver.

- The linear, or linearised, PA ensures an ideal transfer of the RF modulation from the DAC to a high-power signal suitable for transmission, with ideally no adjacent channel emissions. Note that this function could also be provided by an RF synthesis technique, in which case the DAC and power amplifier functions would effectively be combined into a single high-power RF synthesis block.
- Anti-alias and reconstruction filtering is clearly required in this architecture (not shown in Fig. 2
- . It should, however, be relatively straightforward to implement, assuming that the ADC and DAC have sampling rates of many gigahertz. Current transmit, receive, and duplex filtering can achieve excellent roll-off rates in both handportable and (especially) base-station designs. The main change would be in transforming them from bandpass (where relevant) to lowpass designs.

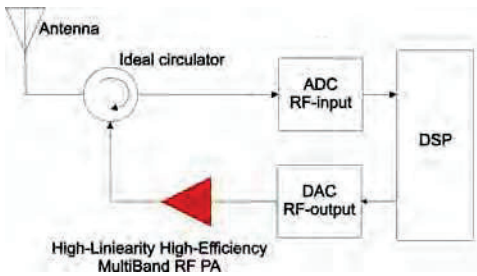

Fig. 2. Ideal software defined radio architecture

Possibly the most important element of any SDR system, whether in a base station or handset, is the linear or linearised multiband transmitter. Receiver systems have always required a high degree of linearity, as they must possess a good signal handling capability, in addition to good low-noise performance. In the case of transmitters, however, a high degree of linearity is a relatively recent requirement, arising predominantly from the widespread adoption of multi symbols envelope-varying digital modulations.

This follows from the fact that most modern modulation formats incorporate some degree of envelope variation, the only significant exception at present being GSM and its derivatives (DCS and PCS). The basic architecture of a SDR transmitter revolves around the creation of a baseband version of the desired RF spectrum, followed by a linear path translating that spectrum to a high-power RF signal.

Nevertheless the implementation of a true SDR poses a further very critical issues, i.e. the power consumption of the analogue-digital converter. Let's consider for instance the use of a flash converter, largely available in the market with a maximum number of bit about 18 preceded by a sample and hold circuit. Carrying out a simplified calculation, given the converter dynamic range, Dc, the power consumption of this systems is:

$$P_{dc} \frac{kT}{t_s} 10^{Dc/10}, \tag{1}$$

Exhibit 1007
Nokia of America Corporation, et al. v. Smart RF Inc.
000054

where the k is the Boltzmann's constant = 1.38×10^{-23} J/K, T is the device temperature and t_s the sampling time. Furthermore the dynamic range of the converter is given by:

$$D_c = 6.02N + 1.76 - PAR + 10\log_{10}\left[2OSR\right], \tag{2}$$

where number of bit, N, a peak-average ratio for the signal, PAR, and an oversampling ratio, OSR. From this easy calculation we can straightforwardly estimate the AD power consumption Pdc in a significant scenario for SDR. Assuming to digitize a frequency band from 800 MHz to 5.5 GHz with a 11GS/s ADC and assuming that the receiver dynamic range is from -20 dBm to -120 dBm, with a SNR of 12 dB at minimum sensitivity, the average PAR of 4, the required N is 20; it results that a such ADC consumes hundred of watt, thus preventing the use of the ideal architecture in Fig. 2. in practical implementation.

4. Reconfigurable Matching Networks

The multiband-multimode demands of today's wireless market, is fulfilled by implementations based on parallel line-ups completed by antenna diplexers and switches to meet the specific requirements of each communication standard, (c.f. Fig. 1). Utilizing only one adaptive transmit path to replace the parallel path concept is conceptually simple, but practical design considerations place severe design constraints and technology. Major challenges consists in creating the tunable filters and PAs [5]. Addressing these challenges means to develop flexible PAs capable to maintain the power-added efficiency (PAE) and linearity while moving among different operating frequencies. In conventional PA implementations, the linearity requirement typically results in the use of class-AB operation for the output, which provides a workable compromise between linearity and efficiency. When considering linearity, the class-AB output stage must be dimensioned in such a way that it can provide its peak output power without saturation. As a result, for a given peak output power and battery voltage, the load impedance for a class-AB stage at the fundamental frequency is fixed to $R_L \approx 0.5 \cdot V_{cc}^2 / P_{Peak}$ .Unfortunately, class-AB operation provides its highest efficiency only under maximum drive conditions. When operated at the required back-off level, due to linearity reasons for a given communication standard, a rather dramatic loss in efficiency occurs. For these reasons improving amplifier efficiency, while maintaining linearity, is currently a major research topic in wireless communications. In linearity-focused researches, the circuit is designed so that the resulting overall linearity performance of the PA module is improved. In this way, the active device can be operated closer to its peak-power capabilities and still be able to meet the linearity requirements.
Techniques that address the efficiency in the back-off mode are dynamic biasing or regulation of the supply voltage of the output stage

[6]. Dynamic biasing provides only modest improvements in efficiency, and supply voltage regulation requires an efficient DC-to-DC conversion, increasing system cost and complexity and operative bandwidth. Nevertheless this techniques appear very promising for future transmitter architectures. An alternative for improved class-AB efficiency is load-line adjustment as a function of output power using an adaptive or reconfigurable output matching network.
An ideal Reconfigurable Matching Network has to provide:

Exhibit 1007
Nokia of America Corporation, et al. v. Smart RF Inc.
000055

- Low Loss
- High linearity
- High Tuning Speed
- Sufficient impedance coverage
- Low complexity
- Low area usage

Power handling of matching networks is a critical issue in PA applications. To reduce the losses in a matching network, the use of a limited number of reactive elements is mandatory, beside the choice of high Q tunable components. Typically, such a network is based on varactor diodes, PIN-diodes or FET switching of matching elements like inductors, transmission-lines or capacitors, also involving micro electromechanical systems to improve the power handling capability [7].

We can conclude that these integrated adaptive networks will play an important role for the realization of the next generation of adaptive transceivers and this paragraph is aimed to describe the ongoing basic researches on this subject.

4.1 Varactor based switching matching network

Varactor diodes, although characterized by a relatively low Q factor at microwave frequencies, can be a choice for enabling RF tuning. Unfortunately, because of their inherently non linear behavior, their use with modern communication standards (characterized by high peak-to-average power ratios), has to be carefully analyzed according to the specific case considered. In Fig. 3 are shown varactor diode based circuit topologies [5] suited to provide matching tuning overcoming the issue related to the linearity of the electron devices.

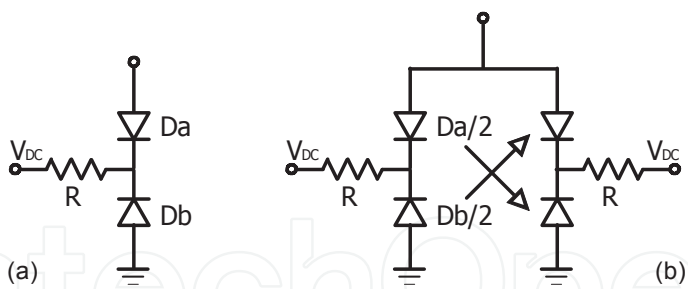

Fig. 3 – (a) Anti-series connection of varactor diodes to minimize third-order distortion, (b) Anti-series/anti-parallel connection of varactor diodes to minimize second and third-order distortion.

Basically, the capacitance of a single varactor diode can usually be expressed as:

$$C(V) = \frac{K}{(\varphi + V)^n} \tag{3}$$

where φ is the built-in potential of the diode, V is the applied voltage, n is the power law exponent of the diode capacitance, and K is the capacitance constant. The power law exponent can exhibit wide variation in different situations, from a value of n≈0.3 for an

Exhibit 1007
Nokia of America Corporation, et al. v. Smart RF Inc.
000056

implanted junction to n≈0.5 for a uniformly doped junction to n≈1.5/2 for a hyper-abrupt junction.
If the applied dc voltage is V_{DC}, then the incremental capacitance of a single varactor diode as a function of the incremental voltage v can be expressed as

$$C(v) = C_0 + C_1 v + C_2 v^2 + \ldots.. \tag{4}$$

where the term C_1 gives rise to second-order distortion and the C_2 term gives rise to third-order distortion. The diode configuration in Fig. 3a can be employed to realize a voltage variable capacitor with theoretically no distortion. Indeed, (referring to the circuit in Fig. 3a) evaluating the expressions for the linear and nonlinear terms of the capacitance, and setting to s the ratio of the diode areas Db/Da, it follows that:

$$\begin{aligned} C_0 &= \frac{sK}{(1+s)(\varphi + V_{DC})^n} \\ C_1 &= \frac{(1-s)nC_0}{(1+s)(\varphi + V_{DC})} \\ C_2 &= \frac{C_0\left[(s^2+1)(n+1) - s(4n+1)\right]}{2(\varphi + V_{DC})^2(1+s)^2} \end{aligned} \tag{5}$$

It can be noted that for n ≥ 0.5, C_2 can be made equal to zero, resulting in zero third-order distortion, by setting

$$s = \frac{4n + 1 + \sqrt{12n^2 - 3}}{2(n+1)} \tag{6}$$

It can be observed from eq. (6), that the particular case of constant doping profile in the diode (the abrupt junction case where n=0.5) results in a value of s=1. This case is particularly attractive because this set of conditions (n=0.5, s=1), sets both C_2 and C_1 equal to zero. A more elaborate analysis shows that all higher order distortion terms also vanish, yielding (in theory) a "distortion-free" operation for this unique case. When dealing with process technologies where n>0.5, eq. (6) provides a direct means of calculating the required diode area ratio to minimize C_2.
For example, in the case where n=1, the required area ratio is exactly two. In the case of n=2, which corresponds to the ideal hyper-abrupt junction, the required area ratio is 2.6.
Although this approach can minimize C_2, it is clear from eq. (5), that a value of s≠1 will result in a finite value of C_1. In this case, a relatively high third-order distortion product will unfortunately still arise, resulting from the secondary mixing of the fundamental with the second-order non-linearity C_1. Fortunately, this distortion contribution can be eliminated, by placing an identical varactor stack in anti-parallel configuration (see Fig. 3b).
The linear capacitance of the circuits of Fig. 3a and b are identical, but the circuit of Fig. 3b has C_1=C_2=0 when the proper area ratio is set. It must be underlined that, in this configuration (Fig. 3b), all the even-order coefficients are zero (C_1, C_3, C_5, …) in this topology, but the higher coefficients that create odd-order distortion (C_4, C_6, C_8, …) are not

Exhibit 1007
Nokia of America Corporation, et al. v. Smart RF Inc.
000057

zero, although the IM3 contributions due to the 5th and higher order nonlinearities are very small.

The implications of this analysis can be summarized as follows:

- The classical configuration of Fig. 3a provides theoretically a "distortion-free" varactor stack when n=0.5, corresponding to a uniform doping profile of the varactors.
- The more generalized configuration of Fig. 3b provides an ultra-low distortion varactor stack for any value n>0.5, by setting the proper ratio of the diode areas, which sets C_1 and C_2 to zero, providing more freedom for use in different process technologies.

It must be underlined that each of the circuits in Fig. 3 requires a very high tap impedance (R) for proper operation. A high tap impedance, limits the impact that forward biasing of one of the diodes by RF signal has on linearity.

An effective way to implement the high impedance while keeping the RC time limited for the control signal is the anti-parallel diode pair depicted in Fig. 4.

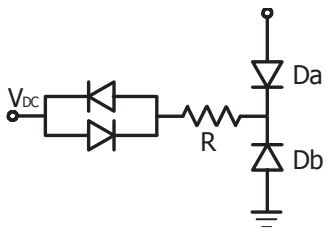

Fig. 4.– Anti-series connection of varactor diodes with modified center tap.

Analyzing, by a two tone test the described matching and comparing them with a single varactor diode we can observe the linearity of the different topologies. The IM2 and IM3 distortion of the circuit in Fig. 3a are comparably low, while the IM3 of the circuits in Fig. 3b is limited by fifth-order distortion due to complete cancellation of the third-order products. In this case indeed, a 1:5 slope dependence for the IM3 components can been found [8], confirming the elimination of the C_1 and C_2 contributions.

Fig. 5 – (a) Equivalent circuit of the "tunable inductor", (b) Simplified circuit of a varactor-based "tunable inductor".

A different option for the implementation of reconfigurable matching network is to act directly on the inductance value, rather than the value of the capacitors as discussed hereinabove. For this purpose varactor diodes can be exploited to create a "tunable inductor" [9]. By considering the circuits in Fig. 5, the equivalent impedance Z of the LC circuits can be written as:

$$Z = \frac{1 - \left(\omega/\omega_c\right)^2}{j\omega C} \tag{7}$$

Exhibit 1007
Nokia of America Corporation, et al. v. Smart RF Inc.
000058

where $\omega_c = 1/\sqrt{LC}$ is the resonant frequency of the circuit. When the condition $\omega > \omega_c$ is achieved, the impedance Z represents an equivalent inductor L_{eq}, that, for the simplified circuits in Fig. 5, is analytically expressed as:

$$L_{eq} = \frac{\left(\omega/\omega_c\right)^2 - 1}{\omega C} \tag{8}$$

The resulting equivalent inductor is a "tunable inductor" whose value is related to the varactor capacitance C (and also ω_c). In Fig. 5b, the varactor parasitic elements have not been represented, however they have to be taken into account during the design of the "tunable inductor".

4.2 Switching matching networks

If the output power of the PA is so high to make the use of varactor diodes prohibitive, a possible solution could be to replace the varactor diodes with fixed value capacitors controlled by switching PIN diodes. By observing to the examples in Fig. 6, if the PIN diode connected to the capacitor is in the ON state, the capacitor adds its own capacity to the global circuit. On the other hand, if the PIN diode is in the OFF state, the capacitor does not affect the global circuit.

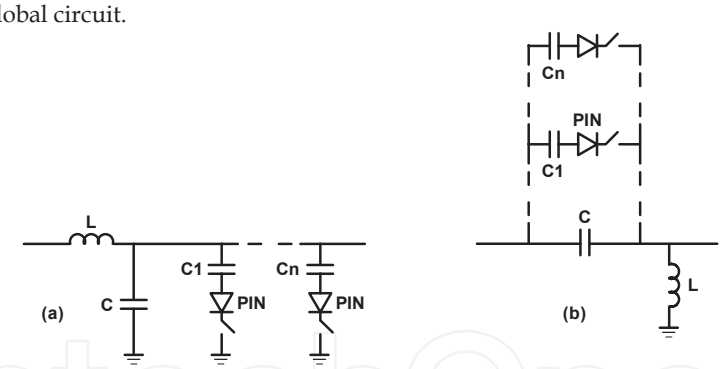

Fig. 6.– (a) Low-Pass Matching Network example, (b) High-Pass Matching Network Example

By using a set of digital signals that change the state of the PIN diodes to active or inverse condition, it is possible to generate $N=2^n$ impedances (where n is the number of PIN diodes used). Unfortunately, such a technique permits only a discrete set of tuning possibilities, resulting inappropriate where fine tuning is requested, unless a considerable number of components is used, thus increasing losses, area usage and costs. A different option of switched matching network is based on MOS devices . The use of MOS devices rather than PIN diodes makes them more suitable for IC designs. The operative principle of the network is discussed by a following example.

Let's consider a Si-Ge HBT device, the optimum fundamental loads at one dB compression point are 15 Ω at 2.45 GHz and 5 Ω and 3.5 GHz respectively, the reactive parts are

Exhibit 1007
Nokia of America Corporation, et al. v. Smart RF Inc.
000059

negligible. These resistance values have been determinate accounting for the output power level to be supplied by the power amplifier in the two different bands. The aim of the output network consists in synthesizing these loads using a MOS switching network topology, schematically depicted in Fig. 7 and investigating the general features.

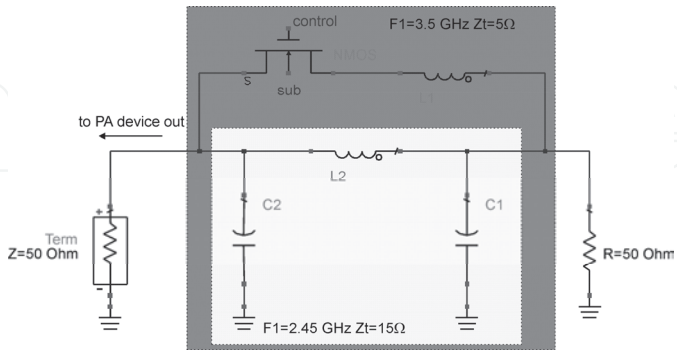

Fig. 7. MOS based switched matching network π topology

The basic simple network topology is based on a π-structure, with an additional branch composed by a NMOS device acting as a switch, with in series an inductor to change the network impedance when the switch is closed. The behavior of the network depends on the switch condition:

1. when the switch is ON (i.e. its R_{ds} value is low, zero in the ideal case) the network should present at its input an impedance value equal to 15 Ω that is the optimum value for the device at 2.45 GHz.
2. When the switch is OFF (i.e. its R_{ds} value is high, infinite in the ideal case) of course, the frequency behavior of the network change. In particular the equivalent value of the inductor between the two shunt capacitors becomes equal to the parallel of L_1 and L_2 and the input impedance of the network decreases to 5 Ω at 3.5 GHz.

Moving on the actual schematic, for the switch it has been necessary to introduce the biasing network in order to guarantee the right switching functionalities. The simulations have been performed biasing the NMOS device, with dc voltages on drain and source set to V_D=3V and V_S=3V respectively, to ensure that the NMOS device is properly biased in the origin of its output characteristics. The gate control voltage is raised to V_G=5V, when the NMOS switch has to realize a short circuit condition, and dropped to V_G=2V when the NMOS switch has to realize an open circuit condition. The feed lines for all three terminals have been realized using 4.8 KΩ resistor for each lines to guarantee the request isolation. Fig. 8 shows the small signal parameters S11 and S21 of the networks, as a function of frequency from 1 GHz to 4 GHz, respectively when the switch is OFF, e.g. when the network has to synthesize the load at 3.5 GHz, and when the switch is ON, e.g. when has to be synthesized the load at 2.45 GHz.

In particular in Fig. 8 left, the blue line in the right part of the figure represents the real part of the input impedance, which can be note is roughly equal to 15 ohm. Unfortunately, the input impedance shows a residual imaginary part due to the non ideal behavior of the inductor and capacitor elements present in the network. Similarly, Fig. 8 right reports the same features when the switch is OFF, e.g. when the network has to realize the load

Exhibit 1007
Nokia of America Corporation, et al. v. Smart RF Inc.
000060

required at 3.5GHz. Also in this case, the network exhibits the requested real part of the input impedance, with a residual imaginary part of the input impedance.

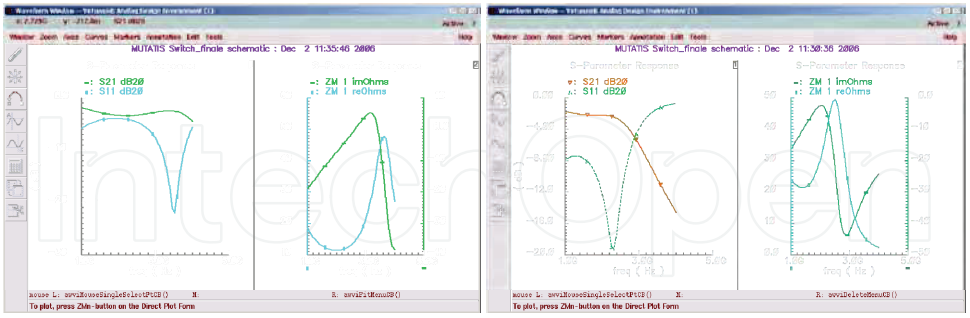

Fig. 8. S11 and S21 frequency behavior together with the real and imaginary parts of the input impedance when the switch is ON (left) and OFF (right).

5. Dual-Band reconfigurable SiGe HBT amplifier design

The above described matching network can been adopted to implement the two matching networks for a class-AB amplifier. In the following example of such design approach is presented. The design of the reconfigurable PA is based on a power device composed of 17x8 elementary SiGe HBT with and emitter area of 8.49 μm². The bias circuitry of the power section is designed to provide other than the required base bias current, a circuit-level linearization. Let's start introducing this latter part, referencing to the Fig. 9. The size of the devices used for the bias circuitry and the values of passive components scale accordingly, so that accurate (i.e. matched) current mirroring can take place. In addition, resistor R4 introduces base ballasting and its value is selected to be 350 Ω per emitter. It helps in reducing the risks due to thermal runaway. A larger value would have better effect, however, that could result in high DC voltage drop at high power drive, and thus early gain compression of T4, the power transistor, would take place.

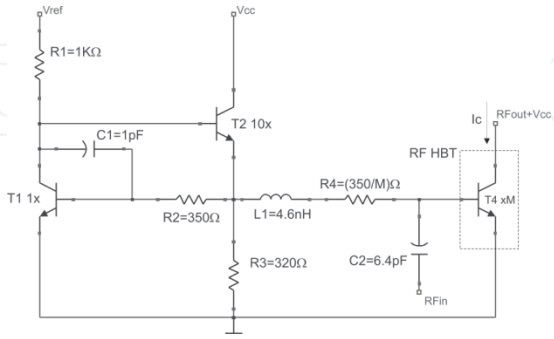

Fig. 9. PA core schematic including the power transistor and the bias network

The power device, which is shown in Fig. 9 within the dotted outline, is biased through the current mirror. By inspection of this figure the current through the reference transistor T1 is:

Exhibit 1007
Nokia of America Corporation, et al. v. Smart RF Inc.
000061

$$I_{REF} = \left(V_{REF} - 2V_{be}\right) \Big/ R1 \quad , \tag{9}$$

with Vbe ~ 0.8 V. If the ratio between the reference device and the RF device is M, in this case M = 17x8, then the current that will flow through the RF transistor is $M*I_{ref}$. in addition, the current mirror behaves like an ideal voltage source, since its output impedance is

$$R_{out} \approx \frac{1}{g_m A_{loop}}, \tag{10}$$

where g_m is the transconductance of the emitter follower device, and A_{loop} is the loop gain of the loop formed by the reference device and the emitter follower (buffer) transistor. At high frequencies, R_{out} becomes inductive and its value should be kept low throughout the frequency band of interest and could be further reduced if resistor R_3 was further reduced in value, at the expenses of an higher current trough this resistor.

At 1 dB compression point, the power transistor should be biased at a collector current which has a value near the optimum value that guarantees that the maximum transition frequency (f_t) of the transistor is achieved. Due to self bias effect, which forces the DC average collector current to increase with increasing input power, the value of the quiescent bias current is chosen to be much lower compared to the value that it reaches under full power drive conditions. So, when the transistor T4 is self biased it starts to draw more current. Since the current flowing through R_2 is constant, as the base-emitter voltage of T_1 is constant, this additional current is supplied by transistor T_2. The capacitor C_1 in the bias network helps to stabilize the loop formed by the reference transistor, T_1, and the emitter follower transistor, T_2. The stability analysis of the loop formed by T_1 and T_2 shown that for unity loop gain the phase margin is approximately 78 degrees, which guarantees the loop unconditional stability. Fig. 10 reports the DC current flowing in the collector of the power device, T4, as a function of the input power at the frequency of 2.45 GHz. From the curve is seen that the quiescent current increases according with the description given above and reaches the value related to the peak f_T, at the 108 mA for an input power of 6 dBm. The value of the bias current for low input power is defined according with the eq. (9), adjusting the value of either R_1 or V_{ref}, in this case to the R_1 = 1 kΩ, corresponds a V_{ref} = 3.3 V.

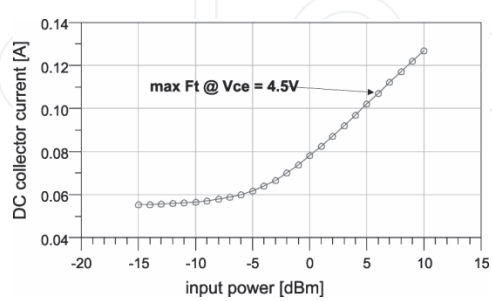

Fig. 10. Behavior of the collector current for the power transistor, T4 in Fig. 9, as a function of the input power at 2.45 GHz.

Exhibit 1007
Nokia of America Corporation, et al. v. Smart RF Inc.
000062

The layout of the reconfigurable PA is illustrated in Fig. 11 (left), where are clearly visible the inductors adopted for the matching and the area for the active part of circuit. The total size of the layout with the bonding pads is 1x1mm. While in operation, the voltage in the node between the inductors swings between positive and negative values. This causes the control MOS drain-bulk np junction to be forwarded biased, which degrades switch performance and may results in latchup. In order to overcome the specific drawback, we set an offset voltage (pin Vofs) which shifts the voltage in the abovementioned node in positive values.

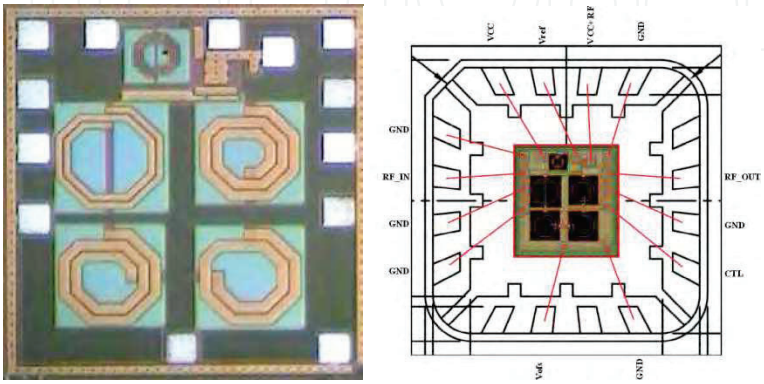

Fig. 11. Layout of the reconfigurable SiGe–PA prototype (left) and its packed wiring diagram (right)

For the design of the inductive part of the matching networks a planar electromagnetic simulator should be used, this permits to calculate any mutual inductances, between the inductors that are in proximity along with the losses in the silicon. Due to the large number of controls and dc-supply for the operation of the components a package is normally required and has to be taken into account during the design. The selected solution consists in the QFN package which allows up to 16 leads. The bonding diagram for this component is reported in the Fig. 11 (right), along with the pin description. At the time of this report editing, the packaged components were not yet available, for the reason the measurement results that will follow consider only the on-wafer device.

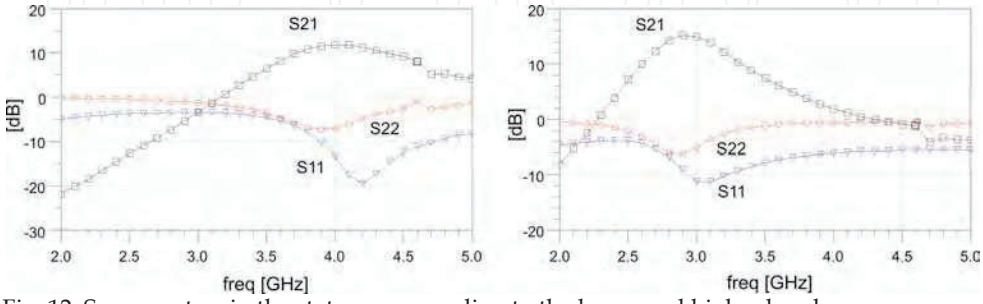

Fig. 12. S-parameters in the state corresponding to the lower and higher bands.

Exhibit 1007
Nokia of America Corporation, et al. v. Smart RF Inc.
000063

The first test of measured data considers s-parameter in the range 2 to 5 GHz. The S21-S11 and S22 in dB for the state corresponding to the lower and higher frequency band are reported in Fig. 12. From the figures is clearly observed the shift in frequency due to the above mentioned reasons, which is estimated in the range of 500 MHz. While the small-signal gain maximum is 2.5 dB lower than the simulated in the lower frequency band and 1 dB less in the higher band. This reduced matching have to be attributed to the matching which, being lower than estimated for the discussed reasons, introduces and matching loss consistent with the reduced gain observed during the characterization phase. We exclude problems related to the measurement set and calibration, although a problem related to measurements, the ringing in the 4.7GHz, was observed.

The characterization of the sample in the large-signal regime is reported in the below figures. It is carried out at the frequencies where the device exhibits the maximum gain and matching in the two states that are respectively at 2.9GHz and 3.9GHz, which correspond to 500MHz frequency shift from the design target as discussed above. The data related to the large signal gain up to the compression are reported in the Fig. 13, respectively for the state corresponding to the lower and higher frequency. In this figure the CW single tone signal is applied in the two states and the Pout-Pin curves are recorded. The value of the gain is consistent with the small-signal gain while the compression point is estimated to be about 16 dBm for the lower band and 15 dBm for the higher frequency. These figures are 1 dB lower that estimated during the simulations. All this data are consistent with the simulation and again supports the hypothesis that introducing the additional inductive parts due to the packaging the proper frequency behavior can be reached.

An intermodulation product characterization considering a two-tone signal with a center frequency at the selected frequencies of 2.9GHz and 3.9GHz and 1MHz offset, was applied to the device. The input power was swept from -10dBm to 13dBm. The results of the characterization, in terms of the higher IM3 are reported in the Fig. 13. It is observed that any consistent change in slope is observed in the traces. This allows concluding that the MOS involved in the switched matching networks doesn't introduce any additional nonlinearities. In fact, if the additional nonlinearity required changing the state of the device, was effectively excited we would have observed an addition component in the IM3. It is also worth to observe that the input power dealt by the device is below the threshold for which this effects become evident. This threshold from simulation is estimated in the range of 28-30 dBm.

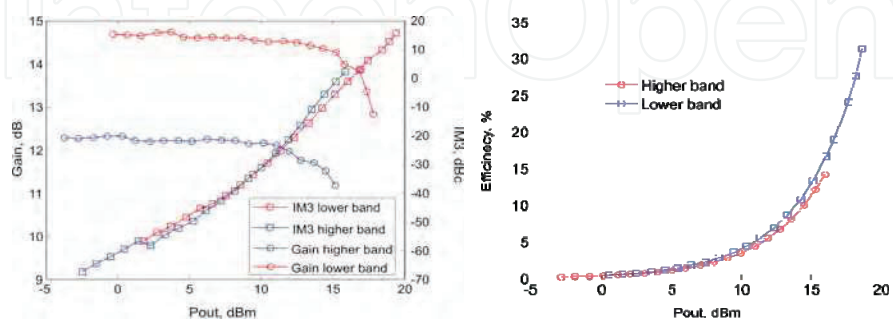

Fig. 13. single tone large-signal gain at 2.9GHz and 3.9GHz and two-tone large-signal inter-modulation offset frequency 1MHz, data reported for the higher IM3 (left), PAE

Exhibit 1007
Nokia of America Corporation, et al. v. Smart RF Inc.
000064

6. Dual-band power amplifier architectures

The main objective of this paragraph is about the consistent and quantitative evaluation of a two possible architectures of dual-band PA both suitable for their involvement in the concurrent dual-band systems, [12]. The first is based on two dedicated PAs combined by a frequency diplexer while the second is specifically designed to be operated in dual-band state. For the sake of the comparison the operative frequency are defined as 1.98 and 3.42 GHz respectively suitable for WCDMA and OFDM radio access technologies.

The two dual-band architectures considered in this paragraph are based on the schematic representations reported in Fig. 14. In the first (Fig. 14, left) the PA is implemented by making use of two dedicated PAs combined by a frequency diplexer. This latter device has to be designed to combine the two PAs introducing band-pass and band-stop behavior in each of the two branches. This is implement by the most innovative technique and technology and it still represents a very critical part of the entire PA structure. Indeed, this component must guarantee an almost lossless behavior in the two transmission paths and as much as possible isolation between them; without sacrificing the matching. In particular the transmission loss characteristic is required to preserve the combined efficiency of the entire structure, while the isolation is a required feature to avoid the cross-modulation between the two dedicated PAs. The constraints on the diplexer become more critical in the case of closer operative spectrum bands. During the two dedicated PAs design, the eventual combination with the diplexer implies a specific additional PA design consideration related to an accurate evaluation of the out-of band termination, which might degrade the output power and efficiency of the two units. The treatment of the harmonic termination of the due to the diplexer is out of the scope for the present treatment.

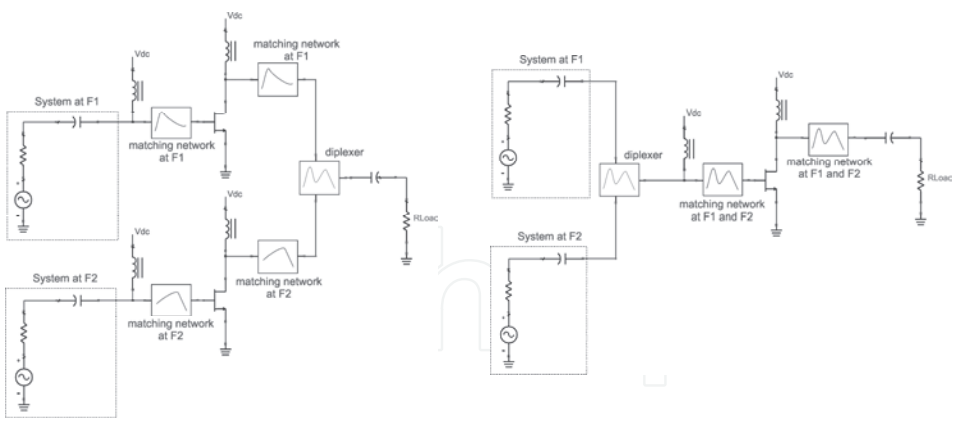

Fig. 14. Schematic of the concurrent dual-band PA implemented by two combined dedicated PAs (left), and by a dual-band PA (right).

Either the dedicated frequency PAs and concurrent PA topology consist of conventional class-AB PA designs, where the tuned matching networks can be synthesized by either passive and\or distributed elements properly dimensioned, without external tuning controls. For the concurrent PA (Fig. 14, right), the two signal sources are combined prior to

Exhibit 1007
Nokia of America Corporation, et al. v. Smart RF Inc.
000065

be applied to the PA input. The design method of concurrent dual-band PA based on multi-tuned networks composed of lumped elements is discussed in [10].

The investigation carried out in this chapter relies on prototypes designed and fabricated using low cost off the shelf active devices along with discrete SMD passive components assembled on FR4 0.8 mm thick evaluation printed circuit board designed with microstrip technology. For this specific test several electron device technology can be considered, eider bipolar or FET fabricated using several different material, spanning from Si to GaAs and possibly GaN. In the present case we choose as active device a GaAs FET, namely the ATF50189 from AVAGO Technologies, a medium power enhanced mode p-HEMT with a cut off frequency of 6 GHz and a 1-dB compression point of 29 dBm at 2 GHz. Optimum bias point for efficiency, linearity and gain can be fund either from manufacturer specifications or CAD simulations, on the basis of nonlinear model analysis. For the specific device possible bias point is found to be 4.5V drain supply voltage with a corresponding quiescent current of 200 mA. The chosen bias point drives the ATF50189 transistor in the AB class operation. The design was based on load and source pull simulations carried out at the two fundamental frequencies of 1.98 and 3.42 GHz, adopting a nonlinear device model which included the package parasitic. Simulations provided saturated output power of 28 dBm and 26 dBm respectively in the lower and higher frequency bands with a power added efficiency of approximately 40% and 35% at the 1-dB gain compression point. The resulting load and source constant power contours are shown respectively in Fig. 15.

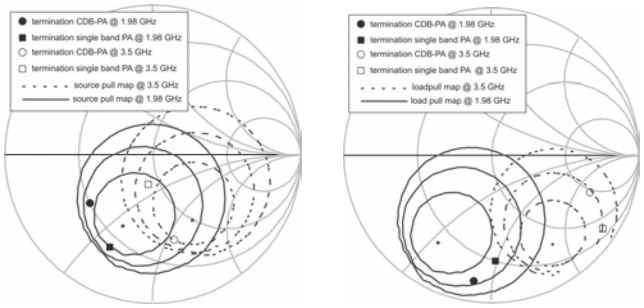

Fig. 15. Simulated source-pull (left) load-pull (right)contours at 1.98 GHz and 3.42GHz, 1 dB steps, and terminations at fundamentals for the single band and dual-band prototypes

The implementation of the source and load terminations defined by the source- and load-pull analysis was obtained by using lumped elements matching networks. This technique, by employing a different approach with respect to standard microstrip technology, enabled the achievement of highly compact prototypes. All the designed PAs adopt the same general topology for the input and output matching networks. Different nominal values and the absence of some of the components determine the difference between the prototypes. In addition, the input network accommodates a stabilizing network which has bee implemented by all three prototypes. The presence of shunt capacitors at both the gate and drain terminals, provide a short circuit to the second harmonic.

Exhibit 1007
Nokia of America Corporation, et al. v. Smart RF Inc.
000066

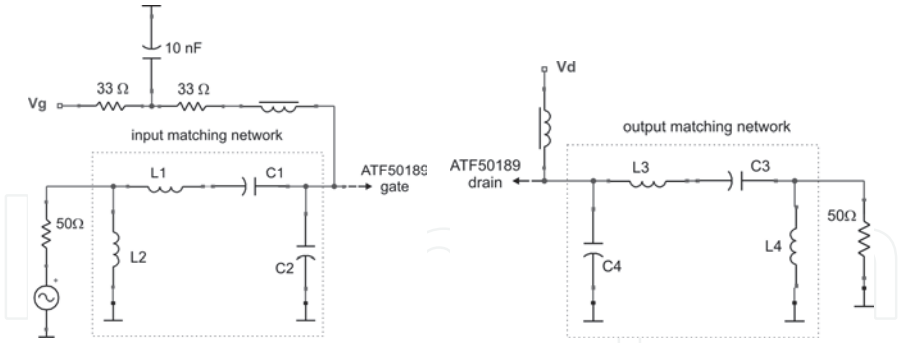

Fig. 16. Prototypes input (left) and output (right) matching network circuit schematic

The selected matching networks pi-topology, exhibits high out of band frequency roll off and a null in the transfer characteristic between the two fundamental frequency bands at 1.98 GHz and 3.42 GHz so enhancing isolation between frequency bands. In order to properly define the networks the additional conditions for maximum efficiency and 1-dB compression output power under large signal excitations were taken into account. To simplify the description we can consider that the three prototypes adopt the same general topology for the input and output matching networks, whose schematics are represented in Fig. 16. As far as the networks dimensioning is of concern, it is possible to show that the 4 unknown (2 inductors and 2 capacitors for each network) are calculated solving a nonlinear system of four equations, where the number of equations results directly equating the two real parts and the two imaginary parts of the equivalent impedance, in symbolic format, with the required optimum impedances. Different nominal values and the absence of some of the components will determine the difference between the prototypes. In addition to matching purpose the input network accommodates a stabilizing network which is common for all the three prototypes. The resulting matching networks result very compact and capable to satisfy the conditions for the optimization of both the output power and gain. The presence of shunt capacitors at both the gate and drain terminals, C2 and C4 in the figures, provide a short circuits at the second harmonics. The resulting best values for the SMD capacitances and inductances are those indicated in Table 1 and Table 1. Input matching network L-C values

respectively for the input and output matching networks. The achieved impedance are reported in the Fig. 16 where the mismatch between the actual values and the optimum impedances for power level take into account for the additional condition of gain and commercial availability of the nominal values.

	C1	L1	C2	L2
concurrent dual band	1.7 nH	0.33 pF	7.6 nH	0.3 pF
single band at 1.98GHz	0.6 nH	1.47 pF	n.a.	n.a.
single band 3.42GHz	1.6 nH	0.26 pF	n.a.	n.a.

Table 1. Input matching network L-C values

Exhibit 1007
Nokia of America Corporation, et al. v. Smart RF Inc.
000067

	C4	L4	C3	L3
concurrent dual band	0.6 pF	3.2 nH	0.77 pF	2.88 nH
single band at 1.98GHz	n.a.	n.a.	1.7 nH	1.9 pF
single band 3.42GHz	n.a.	n.a.	1.1 nH	0.5 pF

Table 2. Output matching network L-C values

The three PA modules were fabricated using FR4 PCB technology and then adopted to implement the two dual-band PA configurations, namely the combined PAs and the dual-band PA. The diplexer used in the large-signal test benches it is realized in microstrip technology and provides an insertion loss of 0.6 dB and 0.8 dB respectively at 1.9 GHz and 3.4 GHz, and isolation between the two channels better than 30 dB and a return loss higher than 20 dB.

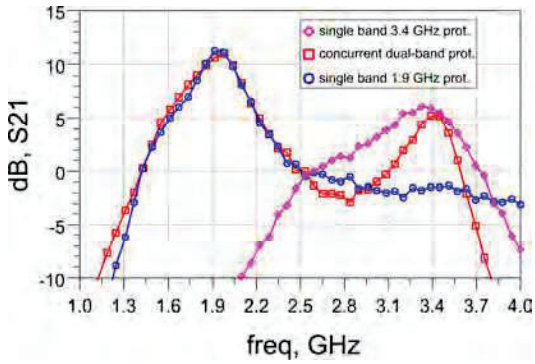

Fig. 17. Measured small-signal gain for the concurrent dual-band and the two single band prototypes

The preliminary test was performed in small signal regime to assess the prototypes performance and to verify the consistency of the comparison. The measured small signal gains associated with the concurrent dual-band PA and with the two single-band PAs prototypes are compared in Fig. 17. The figure indicates that at 1.98 GHz the maximum linear gain is approximately 11dB for both single band and dual band circuits. In the 3.4 GHz band the PA prototypes exhibit a maximum linear gain of 6 dB at 3.42 GHz, and present a 0.5dB gain bandwidth of approximately 60 MHz. Input and output return losses are not reported but are below –15 dB in the respective frequency bands for all the PAs. Small signal characterizations have indicated a very close correspondence between the single band circuits and the concurrent dual band PA in terms of both input/output return loss and gain. This results show that the design of a concurrent dual-band PA using compact lumped elements is feasible without loss of performance at small-signal and makes the characterization and comparison with large and modulated signals meaningful.

The first set of large signal measurements test bench is deployed to fully characterise the PA prototypes with CW large signal excitations. The data are useful to compare the maximum linear power, the gain and the efficiency of the two architectures. In particular the comparison between the power gains as a function of the two CW signals at 1.98 GHz (namely F1) and 3.4 GHz (namely F2), reported in Fig. 18, shows that the combined PA

Exhibit 1007
Nokia of America Corporation, et al. v. Smart RF Inc.
000068

architecture is capable to maintain the two channels mostly separated producing a gain compression which is insensible from the concurrent signal at the side band. In fact the contour plots show a linear behaviour which is independent of the power level in the other channel. At the contrary for the dual-band PA, the mutual interaction between signals at the two frequencies is evidenced by bended constant gain loci, see Fig. 19. Nevertheless, although the effect of the side band is quite evident, the effect of the output diplexer is such that the maximum output power was slightly higher. For example, we can notice that at 1.98 GHz for input power equal to 16 dBm the gain is 8.7 dB for the combined PAs while 9.5 dB for the dual band. This latter condition is maintained only when the input signal at 3.4 GHz is lower than 10 dBm. Similar behaviour is observed in respect to the power gain calculated at 3.4 GHz. From the contour plots it is observed that the loci corresponding to 8.5 dB and 4 dB correspond to the linear gain that the dual-band PA can provide and, consequently, the input ranges which guarantee the linear operation of the PA. Differently, in the case of the combined PAs, the linearity in one frequency band does not depend of the side band.

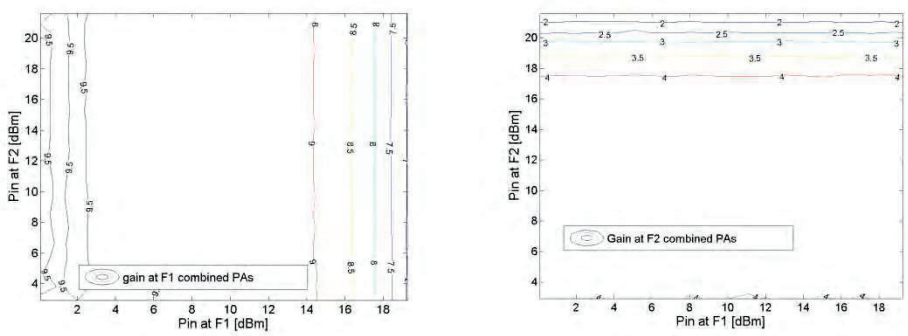

Fig. 18. Power gain [dB] in large signal regime evaluated at the frequency of 1.98 GHz (left) 3.4 GHz (right) as function of input power at 1.98 GHz (F1) and 3.45 GHz (F2), for the combined PAs architecture.

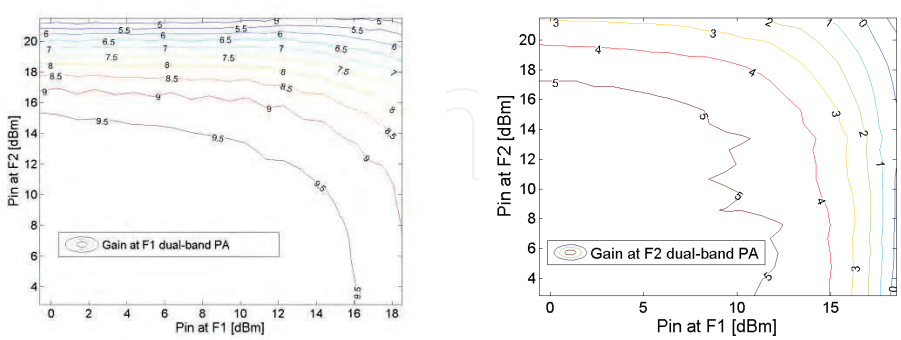

Fig. 19. Power gain [dB] in large signal regime evaluated at the frequency of 1.98 GHz (left) 3.4 GHz (right) and as function of input power at 1.98 GHz (F1) and 3.45 GHz (F2), for the dual-band PA architecture.

Exhibit 1007
Nokia of America Corporation, et al. v. Smart RF Inc.
000069

From the contour plots it is observed in the case of the combined PAs and in the case of the dual band PA, the presence of the diplexer and the mutual interaction between carriers respectively, determine the output power in correspondence of a 1-dB compressed power gain reported in Table 3. This latter consideration leads to the conclusion that from the point of view of the CW output power there are not differences between the two architectures. This latter consideration leads to the conclusion that from the maximum output power in CW condition there are not differences between the two possible architectures.

architecture	1.98 GHz	3.4 GHz
Combined PAs	25 dBm	22 dBm
Dual-band PA	24.5 dBm	23 dBm

Table 3. Simultaneous maximum linear output power (at 1 dB gain compression)

A further very significant figure is represented by the Power Added Efficiency (PAE) for the two PA architectures. In the case of dual-band concurrent PA the PAE is calculated by:

$$PAE = \frac{\left(P_{load}^{F1} - P_{av}^{F1}\right) + \left(P_{load}^{F2} - P_{av}^{F2}\right)}{P_{dc}}, \tag{11}$$

The above equation admits that the two signal are uncorrelated and where P_{dc} takes into account for the total current drawn by the PA modules. The PAE as a function of the input power at the two carrier frequencies, respectively for the combined PAs and the dual band PA architectures are reported in Fig. 20.

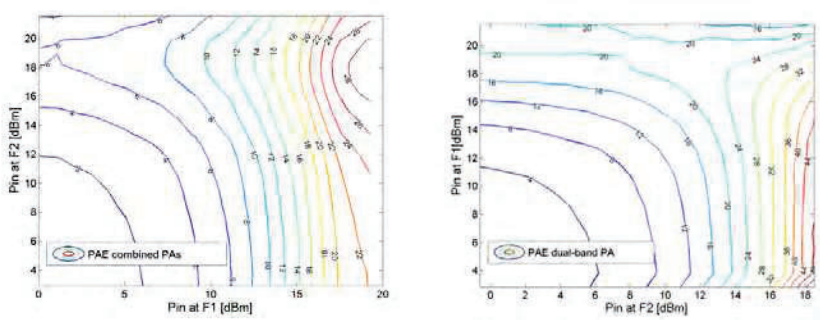

Fig. 20. Power added efficiency [%] in large signal regime as function of input power at 1.98 GHz (F1) and 3.45 GHz (F2), for the combined PAs architecture, (left), and the dual-band PA architecture, (right).

From these experimental verification it is confirmed the intuition that the dual-band PA PAE takes advantage from the current reuse which is inherent in the use of a single power device, when compared with the case of the combined PAs which need twice of the DC power to bias the two PAs. This determine an almost factor 2 in the PAE for the dual-band PA for almost the entire range of evaluation. In particular at 1-dB gain compression the PAE achieved with the combined PAs architecture is in the range of 20%, as evidenced in Fig. 20 left, while in the case of the dual-band PA it reaches 32 %, see Fig. 20 right. The maxima are 28 % and 44% respectively for the combined PAs and the dual band PA architectures. By this figure we can observe a significant improvement of the dual-band PA with respect to

Exhibit 1007
Nokia of America Corporation, et al. v. Smart RF Inc.
000070

the combined PAs architecture. The absolute maximum power for the two PAs are reported in the Fig. 21, calculated by summing the power level at the two carrier frequencies, assumed uncorrelated. Form the contour plots is observed that, regardless linearity concerns, the total power provided by the two systems are slightly the same.

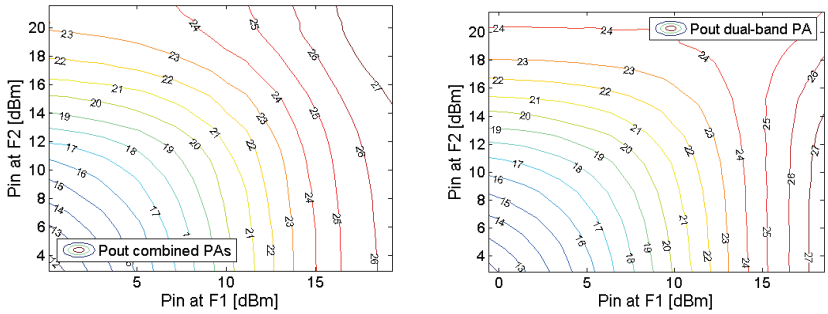

Fig. 21. Total output power [dBm] in large signal regime as function of input power at 1.98 GHz (F1) and 3.45 GHz (F2), for the combined PAs architecture (left) and for the dual-band PA architecture, (right).

The next test concerns about the capability of the dual-band PA architecture to deal with modulated signals and its performance are compared with the combined single band PAs; henceforth the combined PAs architecture is not longer considered. In this case, the base-band signals were down-loaded in the arbitrary signal generators (Agilent ESG 4438C) by using the tools available in the Agilent ADS2006A systems. Two different digitally modulated signals were employed to evaluate PA performance: a 3GPP up-link W-CDMA 3.84 MHz chip rate signal at 1.98 GHz and a 5MHz OFDM 16-QAM signal at 3.42GHz corresponding to one of the WiMAX modes. The output of the PA under test was connected to the VSA (Agilent N9020, 26MHz bandwidth) which was synchronized with the two arbitrary signal generators. The first set of data refers to the large signal gain plotted against the output power for the three PA modules; the comparisons between several operating conditions are shown in Fig. 22, left and right, for the lower and higher frequency bands respectively, which include also CW for the sake of a better comparison.

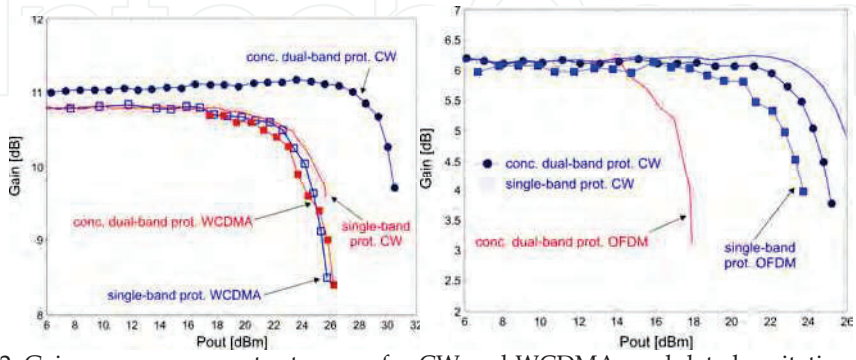

Fig. 22. Gain curve versus output power for CW and WCDMA modulated excitations, both with carrier at 1.98 GHz (left) and 3.42 GHz (right).

Exhibit 1007
Nokia of America Corporation, et al. v. Smart RF Inc.
000071

It is observed that when the amplifiers are driven by a single modulated signal peak power at 1dB gain compression point decreases: this effect is explained by the fact that gain compression in PAs driven by digitally modulated signals occurs at lower power levels than for 1-tone CW signals. In addition, load pull CAD analysis and successive design were performed based on a CW test signal, while experimental results show that the optimum load impedance for maximum linear output power as well as peak efficiency varies depending on the characteristics of the input signal, i.e. pulsed, modulated or CW. Concurrent mode was then operated by simultaneously feeding the dual-band PA with OFDM and WCDMA signals at the two center band frequencies. Reduction of peak output power with respect to single-channel excitations is mainly due to the simultaneous presence of two modulated signals in the same device which cause cross-modulation between the two time varying envelopes. A resulting 4 dB and a 4.5 dB peak power reduction at 1.98 GHz and at 3.42 GHz respectively were measured with respect to the single channel cases.
Moving on to system level figures, the 5.6% EVM WiMax standard limit and a minimum ACPR of 33dBc for a WCDMA signal as settled by the 3GPP specifications have been taken as a reference for power and efficiency values. The goal of the large signal characterisation has so being focussed on the evaluation of the peak output powers and the resulting PAE levels achievable in the two frequency bands with both concurrent dual-band and single-band excitations so as to satisfy EVM and ACPR constrains.

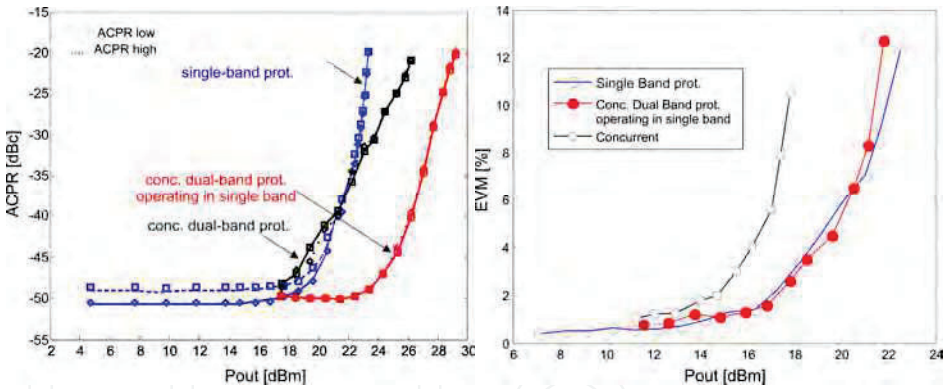

Fig. 23. (Left) Adjacent channel power ratio measured at 5 MHz offset and integrated over the bandwidth, for the single band and the dual-band prototypes with the WCDMA signal at 1.98 GHz; (Right) Error vector magnitude measured for the single band and the dual-band prototypes with the OFDM signal at 3.42 GHz.

From Fig. 23 it is observed that at 1.98 GHz the maximum achievable output power, due to ACPR constrains, is 27.5 dBm when the dual-band PA is working in single-channel mode, while for the concurrent dual-band case this limit decreases to 23 dBm. Data in Fig. 23 show EVM versus the output power results, for single channel operation and dual band mode at 3.42 GHz: a maximum output power of 20 dBm is achieved in the first case while when the dual-band PA is working in concurrent mode, maximum output power settles to 17 dBm. The above data indicate that a significant change in performance arises when the PA is driven in the concurrent dual band mode, specifically resulting in a peak power back off of about 4.5 dB and 3dB respectively for the lower and higher frequency bands due to meet the

Exhibit 1007
Nokia of America Corporation, et al. v. Smart RF Inc.
000072

EVM and ACPR restrictions. Envelope cross-modulation and inter-modulation explain the EVM and ACPR increased growth with input power when compared with single channel mode. Experimental data showed that a 2 dB back-off is necessary with concurrent operation to maintain the EVM at 4.1%. It can be concluded that the proposed solution is capable to provide the same system level performance of more conventional solutions while increasing the overall PAE and allowing a significant reduction of the system complexity.
A further implementation of dual band PA in GaN technology can be found in [13].

7. Dual-band power amplifier digital linearization

As discussed in the above paragraphs, the application of digitally modulated signals to a PA, which is considered hereinafter as an nonlinear (NL) dynamic system, causes in-band distortion and spectrum spreading and finally determine a degradation of the signal quality. The most effective broadband linearization systems have usually been based upon the feedforward technique [14]. However, RF and baseband predistortion linearization techniques have become an attractive solution owing to their reduced cost and complexity.
For multicarrier PA applications, an effort has been placed to increase the bandwidth of predistortion linearization to combat fast memory effects. Baseband Digital Predistortion (DP) seems to be the most promising one. It works by the introduction, in the digital baseband, of an opposite NL of the PA's one, allowing for greater efficiency through a significant power backoff reduction. The most of the available DP techniques deal with single-band operation, although recently an approach to deal with multi-carrier and potentially for multiband systems was presented in [15]. In this technique the modulation bandwidth in several bands and then a DP algorithm is applied selectively the inband and interband third-order intermodulation distortion (IMD3) As the approach relies on third order Volterra model the accuracy of the DP depends upon the identification procedure and the frequency band spacing.
Here we discuss a novel method of Dual Band DP (DB-DP), based on the simultaneous predistortion of both channels at intermediate frequency (IF), [16]. The proposed method uses a single band memory polynomial DP for linearization. As a feedback path we propose a subsampling receiver.

7.1 Basic principles of digital linearization

Let's start reviewing the basic concepts of the DP system. It consists basically in the introduction, at the baseband, of a subsystems which has a transfer function which is opposite to the one of the PA, as in Fig. 24.

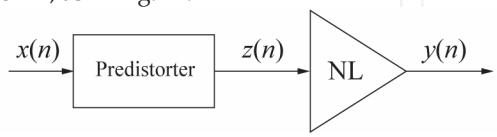

Fig. 24. Predistorsion Principle applied to a nonlinear system

The predistorter can be Look-Up Table (LUT) based or polynomial-based: in the first case, a LUT indexed by the input power is filled with complex coefficients, and the input $x(n)$ is multiplied with the corrisponding one; in the second, the complex coefficients of a k-order

Exhibit 1007
Nokia of America Corporation, et al. v. Smart RF Inc.
000073

polynomial approximating the inverse of the PA's characteristics are found, and the DP output $z(n)$ is given by:

$$z(n)=a_1x(n)+a_2x(n)+a_3x(n)+\cdots \tag{12}$$

The coefficients vector a can be found through a recursive algorithm based on the Indirect Learning architecture shown in Fig. 25. The name derives from the fact that the polynomial coefficients are found without passing by the determination of the PA's characteristics.

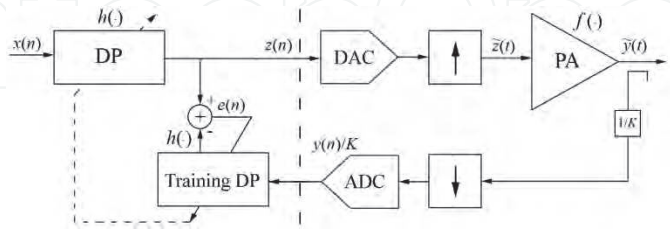

Fig. 25. Indirect Learning schematic principle for a DPD system

The indirect learning techniques works by two identical predistorters, the first – the actual one – in the transmission path and the second – the training one – in the feedback path. The outputs of both are compared to produce an error signal:

$$e(n)=\hat{z}(n)-z(n) \tag{13}$$

where $\hat{z}(n)$ is the output of the training DP. It can be demonstrated that when the error energy is zero the PA's baseband output $y(t)$ is linear with the baseband input $x(n)$, that is the cascade of predistorter and amplifier becomes linear. If the PA's memory length is comparable to the envelope variations of the signal, the baseband model – which we call memory polynomial – can be adopted:

$$y(n)=\sum_{\substack{k=1,\\ k\ \text{odd}}}^{K}\sum_{l=0}^{L-1} b_{k,l}\ z(n-l)\left|z(n-l)\right|^{k-1} \tag{14}$$

where K represent the order of the DP, while L is the number of memory samples; the baseband equivalent input $z(n)$, the output $y(n)$ and the coefficients $b_{k,l}$ of the model, are all complex valued in general. The predistorter's output can be written the same way:

$$z(n)=\sum_{\substack{k=1,\\ k\ \text{odd}}}^{K}\sum_{l=0}^{L-1} a_{k,l}\ \mathrm{x}(n-l)\left|x(n-l)\right|^{k-1} \tag{15}$$

It has to be equal to the Training DP's output $\hat{z}(n)$ to minimize the error energy, that is:

$$z(n)=\sum_{\substack{k=1,\\ k\ \text{odd}}}^{K}\sum_{l=0}^{L-1} a_{k,l}\ \frac{\mathrm{y}(n-l)}{K}\left|\frac{\mathrm{y}(n-l)}{K}\right|^{k-1} \tag{16}$$

The objective consists in finding the parameters $a_{k,l}$ that define the predistorter. Since $z(n)$ is linear in the $a_{k,l}$, the latter can be estimated by a simple least-squares method. By defining a new sequence:

Exhibit 1007
Nokia of America Corporation, et al. v. Smart RF Inc.
000074

$$u_{k,l}(n) = \frac{\mathrm{y}(n-l)}{K}\left|\frac{\mathrm{y}(n-l)}{K}\right|^{k-1} \tag{17}$$

we can rewrite $z(n)$ in matrix form as:

$$\mathbf{z} = \mathbf{U}\mathbf{a} \tag{18}$$

where $\mathbf{z}=[z(0),\cdots,z(n-1)]^T$, $\mathbf{U}=[\mathbf{U}_0,\cdots,\mathbf{U}_L]$, $\mathbf{U}_l=[\mathbf{u}_{1l},\cdots,\mathbf{u}_{Kl}]$, $\mathbf{u}_{kl}=[u_{kl}(0),\cdots,u_{kl}(N-1)]^T$ and $\mathbf{a}=[a_{10},\cdots,a_{K0},\cdots,a_{1Q},\cdots,a_{KQ}]^T$. The least-squares solution for $\mathbf{a}$ is given by:

$$\mathbf{a} = [\mathbf{U}^H\mathbf{U}]^{-1}\mathbf{U}^H\mathbf{z} \tag{19}$$

where $(\cdot)^H$ denotes complex conjugate transpose. A direct implementation of the polynomial predistorter is difficult, because it requires several sample-per-sample multiplications and power raisings. However, an efficient implementation is possible by observing that (15) is equivalent to:

$$\begin{aligned} z(n) = &\left[\sum_{\substack{k=1,\\ k\ \text{odd}}}^{K} a_{k,0}\ \left|x(n)\right|^{k-1}\right]\mathrm{x}(n) + \left[\sum_{\substack{k=1,\\ k\ \text{odd}}}^{K} a_{k,1}\ \left|x(n-1)\right|^{k-1}\right]\mathrm{x}(n-1) + \cdots \\ &+ \left[\sum_{\substack{k=1,\\ k\ \text{odd}}}^{K} a_{k,L-1}\ \left|x(n-L+1)\right|^{k-1}\right]\mathrm{x}(n-L+1) \end{aligned} \tag{20}$$

The nonlinear polynomial can be implemented with a LUT indexed by the input magnitude, $\left|x(n-l)\right|$ [1]. This way, only L complex multiplications per sample are needed. LUT coefficients calculation is performed once the $a_{k,l}$ are found. The performance of the memory polynomial-LUT predistorter depends on the number of quantization points, on the memory length L and on the order of the polynomial, K.

7.2 Sub-sampling receiver

A key component for the DB-DP is the sub-sampling receiver, it operates on the principle of the band-pass sampling theorem, and it is used as feedback path of the DP system. If RF signals have a narrow bandwidth B, they can be sampled with a frequency:

$$f_s \geq 2B \tag{21}$$

As a result of the sampling process, spectrum aliases are generated around all the multiples of f_s as in Fig. 26. The image that falls in $[0; f_s/2]$ (first Nyquist zone) is the exact representation of the input signal, unless a potential phase inversion, and can be digitized.

The same principle can also be used to convert two (or more) band-pass signals s_1 and s_2, located at different carrier frequencies f_{c1} and f_{c2}, with band-widths B_1 and B_2. With a proper sampling frequency there will be replicas of the two signals located side-by-side in the first Nyquist zone with no overlap, as shown in Fig. 27. The proper sampling frequency respect the condition:

Exhibit 1007
Nokia of America Corporation, et al. v. Smart RF Inc.
000075

$$f_s \geq 2(B_1 + B_2) \tag{22}$$

That is, a Nyquist Zone must be wider than the sum of the two bands.

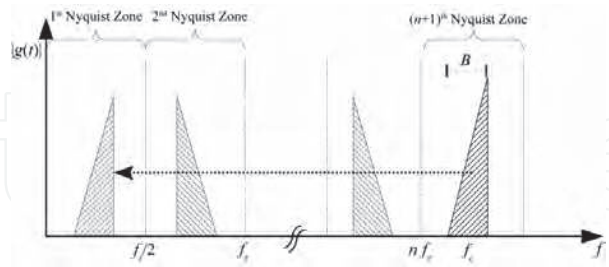

Fig. 26. Single band band-pass sub-sampling principle

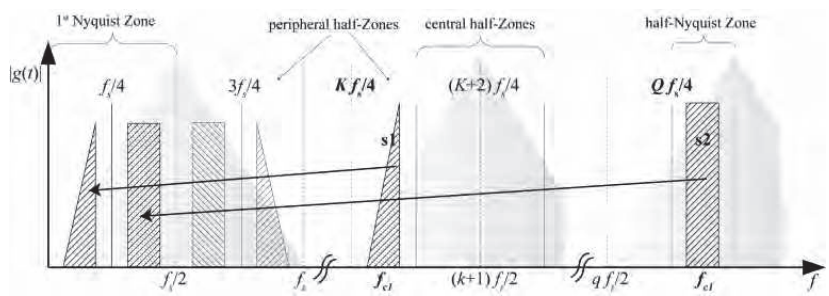

Fig. 27. Dual band sub-sampling principle

The condition of no overlap consists of the both signals to be comprised in a single half-Nyquist zone, i.e. $[nf_s / 4;(n+1)f_s / 4]$, where n is integer. If we define:

$$K = floor\left(\frac{f_{c1} - B_1 / 2}{B_1}\right) \quad Q = floor\left(\frac{f_{c2} - B_2 / 2}{B_2}\right) \tag{23}$$

where $floor()$ is the operation of rounding to the lower integer, the conditions of no overlap are first given by:

$$\begin{cases} kf_s / 4 + B_1 / 2 \leq f_{c1} \leq (k+1)f_s / 4 - B_1 / 2 \\ qf_s / 4 + B_2 / 2 \leq f_{c2} \leq (q+1)f_s / 4 - B_2 / 2 \\ k \leq K \\ q \leq Q \end{cases} \tag{24}$$

where k and q are integers identifying the order of the half-Zone in which the first and the second signals stand, respectively. The other condition, i.e. standing in central vs. peripheral half-zones, are given by:

Exhibit 1007
Nokia of America Corporation, et al. v. Smart RF Inc.
000076

$$\begin{cases} K = 4n \;\Leftrightarrow\; Q \neq 4n, 4n-1 \\ K = 4n-1 \;\Leftrightarrow\; Q \neq 4n, 4n-1 \\ K = 4n+1 \;\Leftrightarrow\; Q \neq 4n+2, 4n+1 \\ K = 4n+2 \;\Leftrightarrow\; Q \neq 4n+2, 4n+1 \end{cases} \tag{25}$$

These conditions lead to a not closed form formulation which require an iterative approach for the solution. Once the suitable sampling frequency is found, the two signals replicas in the first Nyquist zone are located at the frequencies f_{bb1} and f_{bb2} which are given by:

$$\begin{aligned} f_{bb1} &= \begin{cases} f_{c1} - floor(k/4)\cdot f_s & k = 4n, k = 4n+1 \\ \left(floor(k/4)+1\right)\cdot f_s - f_{c1} & k = 4n+2, k = 4n-1 \end{cases} \\ f_{bb2} &= \begin{cases} f_{c2} - floor(q/4)\cdot f_s & q = 4n, q = 4n+1 \\ \left(floor(q/4)+1\right)\cdot f_s - f_{c2} & q = 4n+2, q = 4n-1 \end{cases} \end{aligned} \tag{26}$$

The distortion introduced by a sub-sampling receiver is due in large part to the transfer function of the sampling device. In general, a T/H is preferred over a S/H, because of the lower distortion and higher sampling frequency reachable. The transfer function of a T/H is:

$$G_s(f) = \sum_{n=-\infty}^{\infty} G\left(f - \frac{n}{T_s}\right)\left[\frac{\tau}{T_s}\operatorname{sinc}\left(\tau f\right)e^{-j\pi\tau f} + \frac{T_s - \tau}{T_s}\operatorname{sinc}\left(\frac{n(T_s-\tau)}{T_s}\right)e^{-j\pi(T_s+\tau)\frac{n}{T_s}}\right], \tag{27}$$

where T_s is the sampling period and τ is the length of the hold period. Due to the $\operatorname{sinc}()$ in order to avoid an amplitude distortion, τ should be as low as possible to move at high frequency the first null. Also, the baseband aliases should be as near as possible to the zero. As regards the phase, different replicas have a different offset depending on the order n and the frequency of the alias. Replicas falling into the first Nyquist zone have a phase offset depending on k and f_{BB1}, or q and f_{BB2}. This offset must be compensated if a synchronism between the two signals is necessary, as in our proposed Dual Band DP method.

This approach exhibits some critical points, [17]. The first ones to be considered are noise aliasing and aperture jitter; then out-of-bands signals and wideband noise must be filtered out before the sampler. That noise would otherwise, after sampling, translate and accumulate into the first Nyquist zone. Besides, as even a perfect filter would reject the noise introduced by downstream circuits, low noise components have to be chosen. However, noise aliasing reduces with sampling frequency increase. Aperture jitter can be treated as a white noise if the jitter is low, and it doesn't depend on the sampling frequency. When designing a sub-sampling receiver, another important parameter to take care of is the analog bandwidth of the sampler, that must be greater than the highest frequency of the RF signals.

7.3 Dual Band Digital Predistortion Architecture

The DP-DP is achieved by a RF-level predistortion: a signal predistorter (as opposed to a data predistorter) is able to treat any kind of signal, that is it doesn't depend either on the

Exhibit 1007
Nokia of America Corporation, et al. v. Smart RF Inc.
000077

bandwidth or the center frequency. Let's consider an input signal made of the superposition of two signals at different center frequencies, that is $x(n) = x_1(n) + x_2(n)$. The input is predistorted ($z(n)$), converted into analog ($\tilde{z}(t)$) and amplified ($\tilde{y}(t)$). A portion of $\tilde{y}(t)$ is drawn to have a feedback signal and to train the DP. A scheme is shown in Fig. 28. The main problem with this setup is the lack of sufficiently fast D/A and A/D converters, that will remain so in the foreseeable future because ADC dynamic range and conversion are known to progress at a rate much slower than Moore's law. Also, a RF predistortion is not possible at the moment, because it must be performed sample-per-sample and the sample rate is at least twice the maximum RF frequency (baseband sampling theorem).

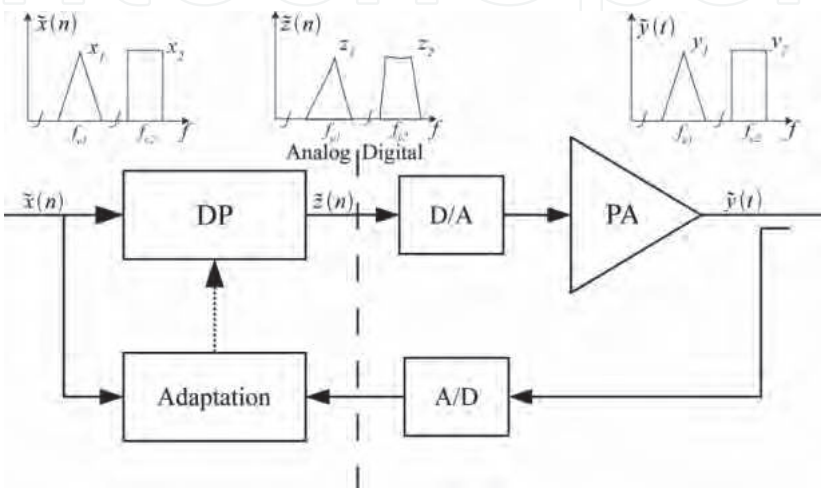

Fig. 28. RF DB-DP, principle of operation

Actually, the converters related problem can be easily overcome. The RF DAC can be replaced by two baseband DAC preceded by a proper digital filtering and digital frequency conversion system. In a similar way, the RF ADC can be replaced by two frequency converters and two baseband ADCs.

There remains the sample rate problem. The last limit can be overcome by introducing a new architecture which is capable to lowering the sample rate, that is predistorting at intermediate frequency (IF). In this case the baseband digital signals $x_1(n)$ and $x_2(n)$ are shifted to f_{IF1} and f_{IF2} then summed, creating $\tilde{x}'(n)$. This IF signal is predistorted ($\tilde{z}'(n)$), and the two bands are separated and shifted to the baseband to be analog converted. The analog PA's input $\tilde{z}'(t)$ is built by those baseband signals, shifted to the RF frequencies f_{c1} and f_{c2}. It is amplified ($\tilde{y}'(t)$) and a portion of it is drawn to create the feedback signals. As a feedback path we propose a subsampling receiver: the two bands composing $\tilde{y}'(t)$ are aliased side-by-side in the baseband, then digitized by a single ADC. In the digital domain, the bands are separated and shifted to IF, composing the signal $\tilde{y}''(n)$ that will be compared to $\tilde{x}'(n)$.

Exhibit 1007
Nokia of America Corporation, et al. v. Smart RF Inc.
000078

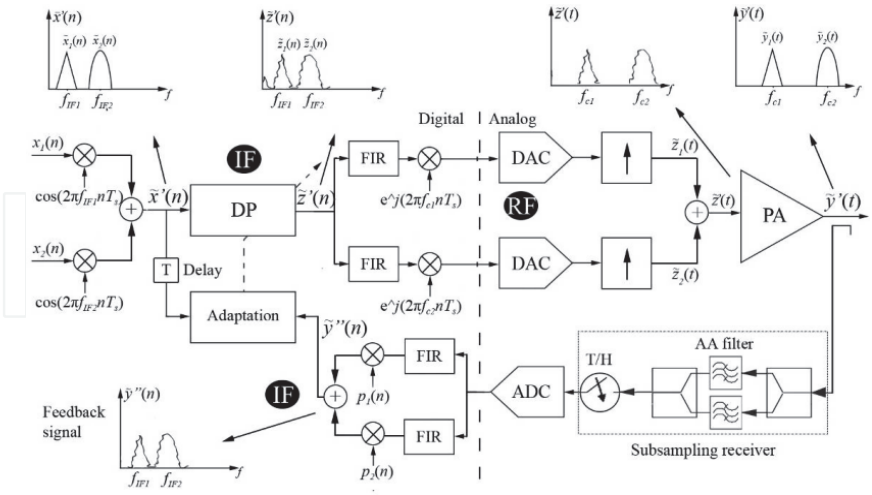

Fig. 29. DB-DP system with IF predistortion and subsampling feedback
The block diagram of the whole system is shown in

When using a subsampling receiver, it is necessary to compensate the different phase offset applied to both bands. This may be done in the digital domain. If a T/H is used, the right phase shift can be calculated through eq. (27). Anti-aliasing filters must be carefully designed with in general out of band rejection. The IFs setting is a crucial point of the system design. They have to be far enough to leave room for out-of-band distortion and to simplify filtering; on the other side, they should be as low as possible to reduce computational constraints. As a rule, for the proposed DB-DP you may consider a sample rate at least four times higher than in a SB-DP system.
The DB-DP was simulated by Matlab/Simulink®. We considered two 16 QAM signals, with amplitudes $P = -10\text{dBm}$ and centre frequencies $f_{c1} = 2.1\,\text{GHz}$ and $f_{c2} = 3.5$ GHz; the sampling frequency was set to $f_s = 146.5\,\text{MHz}$. The PA was modeled with the Wiener-Hammerstein model. LTI blocks preceeding and following the memoryless NL were set to have the following transfer functions:

$$H(z) = \frac{1 + 0.5z^{-2}}{1 - 0.4z^{-1}} \;,\; G(z) = \frac{1 - 0.3z^{-2}}{1 - 0.4z^{-1}} \tag{28}$$

It was chosen a tanh-shaped AM/AM NL, that has G=20dB, IP3=38dB and whose AM/PM is linear, with 5°/dB slope.

Exhibit 1007
Nokia of America Corporation, et al. v. Smart RF Inc.
000079

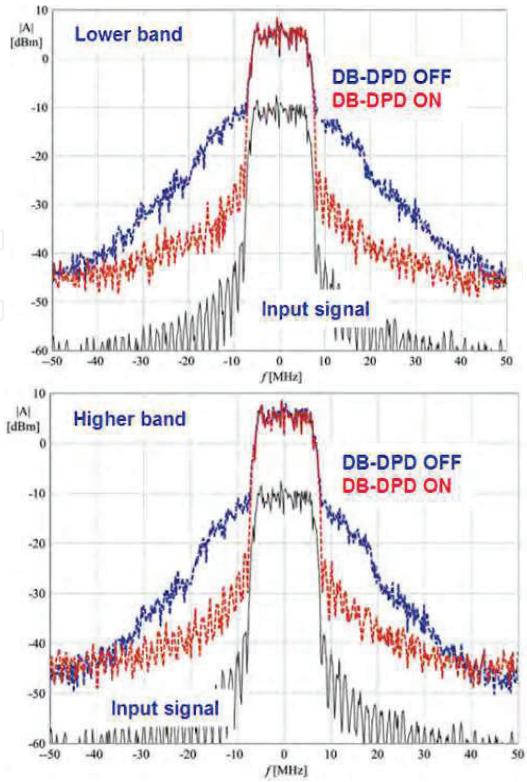

Fig. 30. Spectra comparison for lower and higher channels, between transmitted signal and input signal, with DB-DP OFF and DB-DP ON (left.

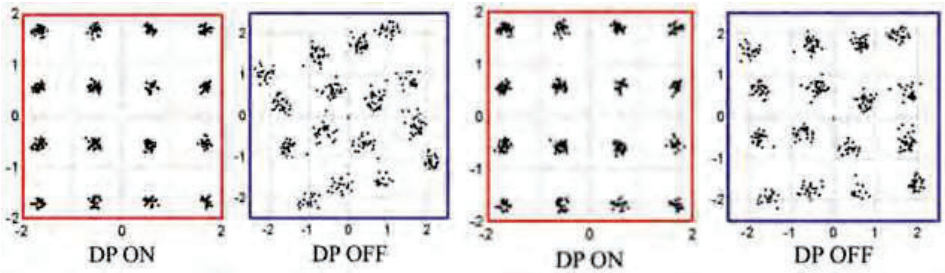

Fig. 31. Constellations comparison for lower (left) and higher (higher) channel, between transmitted signal and input signal, with DB-DP OFF and DB-DP ON

For the implementation of the DB-DPD we used a memory polynomial DP, with a memory length of 4 taps, a polynomial order K=9 and a LUT predistorter with a size of 512. Polynomial coefficients were estimated on a basis of 8192 samples. Simulation results for both channels are shown in Fig. 30 and Fig. 31, where an ACPR and EVM significant reduction is observed. The method proved to be able to correct most NLs, but it is not as

Exhibit 1007
Nokia of America Corporation, et al. v. Smart RF Inc.
000080

good as a SB-DP. While in that case we obtained a Normalized Mean Square Error (NMSE) of 3e-4, in the DB-DP case we obtained an NMSE of 1e-3.

8. Concluding Remarks

The design of flexible PAs and multiband transmitter architectures is at a crucial stage; the number of research teams and projects that approached this field increased over the recent years. The number of special sessions and workshops in the main international conferences confirmed this interest. Some commercial products appeared recently, although they remain mainly based on very simple arrangements of frequency dedicated PAs with limited tuning control. Some technological and methodological problem have to be solved. The first set are related to the device technologies for both the RF power devices and the control devices. Indeed, the energy efficiency and peak power have to be maintained for wideband operation, making the device technology more challenging. Design approach have to take into account for multiband driving which reduce sensibly the power handling capability of the power device. Control devices, like switches and tuning elements have to cope with high peak power increasing the demand of linearity and efficiency, in this field MEMS appears a promising technology. An additional consideration is due for the architectures of multiband-multiband transmitters. Other than flexibility they have to provide excellent signal quality, which is much more threated by simultaneous concurrent signals. Polar transmitters versus Cartesian architectures are investigated as the two mainstreams for future transmitter architectures.

9. Acknowledgement

The contents of this chapter are mainly based on the results of the research activities performed in the context of the project TARGET– "Top Amplifier Research Groups in a European Team" supported by the Information Society Technologies Programme of the EU under contract IST-1-507893-NOE, www.target-net.org.

10. References

[1] Hashimoto, A.; Yoshino, H.; Atarashi, H., "Roadmap of IMT-advanced development," Microwave Magazine, IEEE , vol.9, no.4, pp.80-88, Aug. 2008

[2] F. K. Jondral, "Software-Defined Radio Basics and Evolution to Cognitive Radio", Journal on Wireless Communications and Networking, 2005, vol. 3, 275-283

[3] A. A. Abidi, "The Path to the Software-Defined Radio Receiver", IEEE Journal of Solid-State Circuits, Vol. 42, no. 5, May 2007, pp. 954-966

[4] P. B. Kennington, RF and Baseband Techniques for Software Defined. Radio. Norwell, MA: Artech House, 2005.

[5] J. Laskar, R. Mukhopadhyay, Y. Hur, C. -H. Lee, and K. Lim, "Reconfigurable RFICs and modules for cognitive radio", Digest of Topical Meeting on Silicon Monolithic Integrated Circuits in RF Systems, 2006. Jan. 2006 pp. 18-20

Exhibit 1007
Nokia of America Corporation, et al. v. Smart RF Inc.
000081

[6] F. Wang, D. F. Kimball, J. D. Popp, A. H. Yang, D. Y. Lie, P. M. Asbeck, L. E. Larson, "An Improved Power-Added Efficiency 19-dBm Hybrid Envelope Elimination and Restoration Power Amplifier for 802.11g WLAN Applications," Trans. On Microwave Theory and Techniques, Vol. 54, Dec. 2006, pp. 4086-4099

[7] Q. Shen, N. S. Barker "Distributed MEMS tunable matching network using minimal-contact RF-MEMS varactors," *Microwave Theory and Techniques, IEEE Transactions on* , vol.54, no.6, pp.2646-2658, June 2006

[8]K. Buisman, L.C.N. de Vreede, L.E. Larson, M. Spirito, A. Akhnoukh, T.L.M. Scholtes, L.K. Nanver "Distortion-free varactor diode topologies for RF adaptivity", Microwave Symposium Digest, 2005 IEEE MTT-S International,12-17 June 2005 pp. 157-160

[9]A. Jrad, A.-L. Perrier, R. Bourtoutian, J.-M. Duchamp, P. Ferrari, "Design of an ultra compact electronically tunable microwave impedance transformer", Electronics Letters, Volume 41, Issue 12, 9 June 2005 pp. 707 – 709

[10]P. Colantonio, F. Giannini, R. Giofrè, L. Piazzon, "Simultaneous Dual-Band High Efficiency Harmonic Tuned Power Amplifier in GaN Technology", European Microwave Conference Digest, Munich Oct., 2007

[11] W.C.E. Neo, Yu Lin, Xiao-dong Liu, L.C.N. de Vreede, L.E. Larson, M. Spirito, M.J. Pelk, K. Buisman, A. Akhnoukh, A. de Graauw, L.K. Nanver, "Adaptive Multi-Band Multi-Mode Power Amplifier Using Integrated Varactor-Based Tunable Matching Networks," *Solid-State Circuits, IEEE Journal of* , vol.41, no.9, pp.2166-2176, Sept. 2006

[12] A. Cidronali, I. Magrini, N. Giovannelli, M. Mercanti, G. Manes "Experimental system level analysis of a concurrent dual-band power amplifier for WiMAX and WCDMA applications"; International Journal of Microwave and Wireless Technologies, Cambridge University Press and the European Microwave Association, Vol.1 Special Issue 02, April 2009 pp 99-107

[13]P. Colantonio, F. Giannini, R. Giofre, L. Piazzon, "Simultaneous dual-band high efficiency harmonic tuned power amplifier in GaN technology", European Microwave Integrated Circuit Conference, 8-10 Oct. 2007 pp.127 - 130

[14]R. Meyer, R. Eschenback, and W. Edgerley, Jr., "A wideband feedforward amplifier," IEEE J. Solid-State Circuits, vol. SCC-9, no. 6, pp. 422–448, Jun. 1974.

[15]P. Roblin, S. K. Myoung, D. Chaillot, Y. Gi Kim, A. Fathimulla, J. Strahler, S. Bibyk"Frequency-Selective Predistortion Linearization of RF Power Amplifiers" IEEE Trans on Microwave Theory and Tech., Vol. 56, Jan. 2008, pp 65-76

[16]A. Cidronali, I. Magrini, R. Fagotti, G. Manes, "A new approach for concurrent Dual-Band IF Digital PreDistortion: System design and analysis," Workshop on Integrated Nonlinear Microwave and Millimetre-Wave Circuits, 2008. INMMIC 2008, pp.127-130, 24-25 Nov. 2008

[17]G. Avitabile, A. Cidronali, G. Manes, 'A S-band digital down converter for radar applications based on GaAs MMIC fast sample&hold', *IEE Proceedings-Circuits, Device and Systems, Vol.143, No.6 Dec. 1996 pp.337-342*

Exhibit 1007
Nokia of America Corporation, et al. v. Smart RF Inc.
000082

IntechOpen

IntechOpen

Exhibit 1007
Nokia of America Corporation, et al. v. Smart RF Inc.
000083

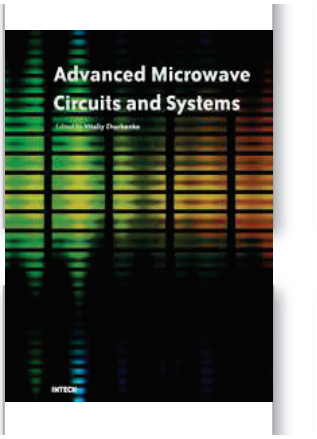

Advanced Microwave Circuits and Systems

Edited by Vitaliy Zhurbenko

ISBN 978-953-307-087-2

Hard cover, 490 pages

Publisher InTech

Published online 01, April, 2010

Published in print edition April, 2010

This book is based on recent research work conducted by the authors dealing with the design and development of active and passive microwave components, integrated circuits and systems. It is divided into seven parts. In the first part comprising the first two chapters, alternative concepts and equations for multiport network analysis and characterization are provided. A thru-only de-embedding technique for accurate on-wafer characterization is introduced. The second part of the book corresponds to the analysis and design of ultra-wideband low- noise amplifiers (LNA).

How to reference

In order to correctly reference this scholarly work, feel free to copy and paste the following:

Alessandro Cidronali, Iacopo Magrini and Gianfranco Manes (2010). Flexible Power Amplifier Architectures for Spectrum Efficient Wireless Applications, Advanced Microwave Circuits and Systems, Vitaliy Zhurbenko (Ed.), ISBN: 978-953-307-087-2, InTech, Available from: http://www.intechopen.com/books/advanced-microwave-circuits-and-systems/flexible-power-amplifier-architectures-for-spectrum-efficient-wireless-applications

INTECH

open science | open minds

InTech Europe

University Campus STeP Ri

Slavka Krautzeka 83/A

51000 Rijeka, Croatia

Phone: +385 (51) 770 447

Fax: +385 (51) 686 166

www.intechopen.com

InTech China

Unit 405, Office Block, Hotel Equatorial Shanghai

No.65, Yan An Road (West), Shanghai, 200040, China

中国上海市延安西路65号上海国际贵都大饭店办公楼405单元

Phone: +86-21-62489820

Fax: +86-21-62489821

© 2010 The Author(s). Licensee IntechOpen. This chapter is distributed under the terms of the Creative Commons Attribution-NonCommercial-ShareAlike-3.0 License, which permits use, distribution and reproduction for non-commercial purposes, provided the original is properly cited and derivative works building on this content are distributed under the same license.

IntechOpen

IntechOpen